Colloquium: Persistent spin textures in semiconductor nanostructures

John Schliemann

Institute for Theoretical Physics, University of Regensburg, D-93040 Regensburg, Germany

(published 5 January 2017)

Device concepts in semiconductor spintronics make long spin lifetimes desirable, and the requirements put on spin control by proposals for quantum information processing are even more demanding. Unfortunately, due to spin-orbit coupling electron spins in semiconductors are generically subject to rather fast decoherence. In two-dimensional quantum wells made of zinc-blende semiconductors, however, the spin-orbit interaction can be engineered to produce persistent spin structures with extraordinarily long spin lifetimes even in the presence of disorder and imperfections. Experimental and theoretical developments on this subject for both *n*-doped and *p*-doped structures are reviewed and possible device applications are discussed.

DOI: 10.1103/RevModPhys.89.011001

CONTENTS

I. INTRODUCTION

The field of semiconductor spintronics emerged around the turn of the millennium and comprises a broad variety of effort toward utilizing the spin degree of freedom of electrons, instead, or combined with, their charge for information processing, or, even more ambitiously, for quantum information processing (Zutic, Fabian, and Das Sarma, 2004; Fabian *et al.*, 2007; Wu, Jiang, and Weng, 2010). Most activities in this area rely on the relativistic effect of spin-orbit coupling described by the Dirac equation and its nonrelativistic expansion in powers of the inverse speed of light c. The well-known spin-orbit coupling term arises here in second order,

$$\mathcal{H}_{\rm so} = \frac{\hbar}{4m_0c^2}\vec{\sigma}\cdot\left(\nabla V\times\frac{\vec{p}}{m_0}\right), \tag{1}$$

where the Pauli matrices $\vec{\sigma}$ describe the electron's spin, m_0 and $\vec{p}$ are its bare mass and momentum, respectively, and V is the potential acting on the particle. Moreover, the free Dirac equation $V=0$ has two dispersion branches with positive and negative energy $\varepsilon(\vec{p})=\pm\sqrt{m_0^2c^4+c^2p^2}$ separated by a gap of $2m_0c^2\approx 1$ MeV, and the nonrelativistic expansion of the Dirac equation can be viewed as a method of systematically including the effects of the negative-energy solutions on the states of positive energy starting from their nonrelativistic limit. Importantly, the large energy gap $2m_0c^2$ appears in the denominator of the right-hand side of Eq. (1) and thus suppresses spin-orbit coupling for weakly bound electrons.

Turning to semiconductors, the band structure of zinc-blende III-V systems exhibits many formal similarities to the situation of free relativistic electrons (as sketched in Fig. 1), while the relevant energy scales are grossly different

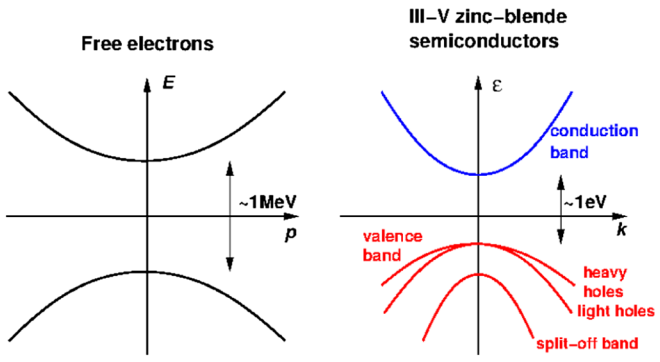

FIG. 1. Left: Dispersion relation of free electrons showing a gap of about 1 MeV between solutions of positive and negative energy. Right: Schematic band structure of III-V zinc-blende semiconductors with a band gap of typically 1 eV. The *p*-type valence band consists of the heavy and light hole branches and the split-off band.

(Yu and Cardona, 2010). For not too large doping, only the band structure around the Γ point matters consisting of a parabolic *s*-type conduction band and a *p*-type valence band with dispersion branches for heavy and light holes and the split-off band. However, the fundamental gap between the conduction and the valence band is of the order of 1 eV or smaller. This heuristic argument makes plausible that spin-orbit coupling is a significant effect in III-V semiconductors and actually lies at the very heart of spintronics research.

A paradigmatic example of a semiconductor spintronics device is the spin field-effect transistor (Datta and Das, 1990) schematically depicted in Fig. 2. In this device proposal, an electron enters a semiconductor region where its spin is rotated via externally manipulable spin-orbit interaction in a controlled way such that the carrier is then transmitted into or, depending on the spin state, reflected from a spin-polarized detector electrode. A shortcoming of this concept is that impurities and other imperfections act as scatterers which change the momentum of the electron (i.e., an orbital degree of freedom) and therefore, again via spin-orbit coupling, easily also randomize the spin, a process known as the Dyakonov-Perel mechanism of spin dephasing (Dyakonov and Perel, 1972). A way to circumvent this effect is to engineer the total spin-orbit field acting on the electron spin in such a way that additional symmetries and related conserved quantities arise which lead to persistent spin structures. This concept has developed many theoretical ramifications and manifested itself in various transport and spectroscopic experiments. These theoretical possibilities and experimental achievements are reviewed in this Colloquium.

This Colloquium is organized as follows: Sec. II deals with persistent spin structures in *n*-doped III-V zinc-blende semiconductor quantum wells and is the main body of this review. In Sec. II.A we introduce the contributions to spin-orbit coupling for quantum wells grown along the high-symmetry directions of the crystal. Section II.B provides a self-contained discussion of the theoretical foundation of conserved spin quantities in [001] quantum wells, but also treats the other high-symmetry growth directions. The semiclassical description of spin densities via diffusion equations and their relation to the persistent spin helix are covered in Sec. II.C. In Sec. II.D we report on the plethora of experiments investigating these predictions along with pertaining further theoretical work. Theoretical results regarding signatures of the persistent spin helix arising from many-body physics are summarized in Sec. II.E. Section II.F is devoted to *n*-doped systems of other geometries including quantum wells of different growth directions and curved structures. In Sec. II.G we summarize developments regarding spin-field-effect transistors and persistent spin textures. Section III contains a discussion of similar persistent spin structures predicted to occur in materials other than *n*-doped zinc-blende semiconductors. We close with an outlook in Sec. IV.

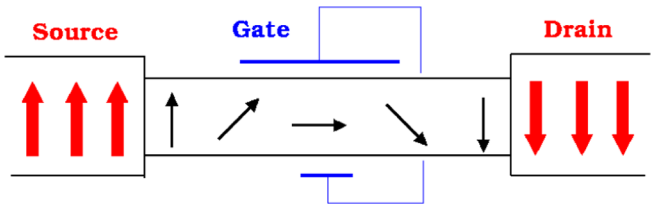

FIG. 2. Schematic of a spin field-effect transistor: An electron is emitted from a spin-polarized source and enters a semiconductor region with spin-orbit coupling being externally controllable via a perpendicular gate voltage. In the above example the spin-orbit interaction reverses the electron's spin during its path, and since the drain electrode is polarized opposite to the source, the conductance of the device is high.

II. *n*-DOPED QUANTUM WELLS

A. Spin-orbit coupling and growth direction

We now summarize important features of the effective description of spin-orbit interaction in zinc-blende III-V semiconductors such as GaAs, InAs, etc., focusing on two-dimensional quantum wells (Winkler, 2003; Fabian *et al.*, 2007; Korn, 2010; Yu and Cardona, 2010). As already mentioned, due to the lower carrier densities in such systems compared to, e.g., metals, we can concentrate on the vicinity of the Γ point, i.e., on wave vectors being small compared to the inverse lattice spacing.

Moreover, we concentrate here on quantum wells grown into the high-symmetry directions [001], [110], and [111] which have been the focus of theoretical and experimental studies so far. However, very recent work by Kammermeier, Wenk, and Schliemann (2016) extended the concepts to be discussed below to more general growth directions.

An important contribution to the effective band structure of three-dimensional bulk systems is the Dresselhaus term given by (Dresselhaus, 1955)

$$\mathcal{H}_D^{\text{bulk}} = \gamma[\sigma^x k_x(k_y^2 - k_z^2) + \sigma^y k_y(k_z^2 - k_x^2) + \sigma^z k_z(k_x^2 - k_y^2)] \tag{2}$$

with the electron's (Bloch) wave vector $\vec{k}$ and a material parameter γ. This contribution is symmetry allowed, $\gamma \neq 0$, due to *bulk-inversion asymmetry*, i.e., the fact that the zinc-blende lattice lacks an inversion center.

In sufficiently narrow quantum wells a simplification occurs as one can, at low enough temperatures, approximate the wave vector components along the growth direction by their average within the lowest subband. For a symmetric well grown along the crystallographic [001] direction we have $\langle k_z \rangle = 0$, and introducing polar coordinates $\vec{k} = k(\cos\varphi, \sin\varphi)$ for the in-plane components it follows (Dyakonov and Kachorovskii, 1986; Iordanskii, Lyanda-Geller, and Pikus, 1994)

$$\begin{aligned}\mathcal{H}_D^{001} &= \beta k(\sigma^y \sin\varphi - \sigma^x \cos\varphi) \\ &\quad - \beta_3 k[\sigma^x \cos(3\varphi) + \sigma^y \sin(3\varphi)]\end{aligned} \tag{3}$$

with $\beta = \beta_1 - \beta_3$ and

$$\beta_1 = \gamma\langle k_z^2 \rangle, \qquad \beta_3 = \gamma \frac{k^2}{4}. \tag{4}$$

Here as before the x and y directions coincide with [100] and [010], respectively. The higher angular harmonics in the second line of Eq. (3) are cubic in k. Neglecting these terms leads to

$$\overline{\mathcal{H}}_D^{001} = \beta(k_y\sigma^y - k_x\sigma^x) \tag{5}$$

which contains a contribution strictly linear in the wave vector ($\propto \beta_1$) and a cubic term ($\propto \beta_3$). The latter is usually a small correction: To give a practical example, for a rectangular well of width $L = 10$ nm we have $\langle k_z^2\rangle = (\pi/L)^2 \approx 0.1$ nm^{-2}. Assuming now a comparatively large density of $n = k_f^2/(2\pi) = 5\times 10^{11}$ cm^{-2} with a Fermi wave vector of $k_f = 0.17$ nm^{-1} (neglecting spin splitting) one finds $k_f^2/4 = 0.007$ nm^{-2}, i.e., $\beta_3(k_f)/\beta_1 = 0.07$. However, there are reports where the quadratic contribution β_3 to the Dresselhaus coefficient β was found to be essential in order to accurately describe experimental data (Walser *et al.*, 2012; Dettwiler *et al.*, 2014). For simplicity we refer to the Hamiltonian (5) as the *linear Dresselhaus term* although it contains cubic corrections.

Quantum wells with other growth directions can be similarly described by appropriately rotating the wave vector and spin in Eq. (2). We restrict the discussion here to the other high-symmetry directions of the cubic lattice (Dyakonov and Kachorovskii, 1986; Eppenga and Schuurmans, 1988). For the [110] direction one finds

$$\mathcal{H}_D^{110} = \frac{\beta}{2}k_y\sigma^z + \frac{3\beta_3}{2}k\sigma^z\sin(3\varphi), \tag{6}$$

where the x and y directions are along $[00\bar{1}]$ and $[\bar{1}10]$, respectively. The coefficient β in the first term is again given by Eqs. (4) as $\beta = \beta_1 - \beta_3$ and summarizes the k-linear contribution and the correction provided by the first-harmonic part of the cubic contributions, whereas the second term contains the third-harmonic part. Remarkably, both terms couple only to the spin projection in the z (or [110]) direction.

The Dresselhaus term for the [111] direction reads

$$\mathcal{H}_D^{111} = \frac{2\beta}{\sqrt{3}}(k_y\sigma^x - k_x\sigma^y) + \frac{4\beta_3}{\sqrt{6}}k\sigma^z\sin(3\varphi) \tag{7}$$

with the x and y directions pointing along $[11\bar{2}]$ and $[\bar{1}10]$. Here the same comments apply as to Eqs. (3) and (6): The first term describes the k-linear part with cubic correction while the second term contains the higher angular-harmonic part of the cubic contributions. Neglecting the third angular-harmonic contributions in Eqs. (6) and (7) leads again to linear Dresselhaus terms incorporating cubic corrections in their parameter β.

The second important ingredient to the effective spin-orbit coupling in quantum wells is known as the Rashba term and is due to *structure-inversion asymmetry*, i.e., it occurs for confining potentials failing to be invariant under spatial inversion along the growth direction (Rashba, 1960; Bychkov and Rashba, 1984). This contribution is described by

$$\mathcal{H}_R = \alpha(k_x\sigma^y - k_y\sigma^x), \tag{8}$$

where the Rashba coefficient α is essentially proportional to the potential gradient across the quantum well and can therefore be varied experimentally. This contribution to spin-orbit interaction is the essential ingredient of the proposal for a spin field-effect transistor due to Datta and Das (1990) already mentioned in Sec. I. The linear Rashba term (8) is independent of the growth direction and invariant under rotations in the x-y plane of the quantum well. Remarkably, the Hamiltonian (8) has the same functional form as the k-linear Dresselhaus term in Eq. (7) for the [111] growth direction.

Although Rashba coupling was first investigated in semiconductors (Rashba, 1960; Bychkov and Rashba, 1984), it is nowadays discussed and studied in a much wider variety of structures lacking inversion symmetry; for a recent overview see Manchon *et al.* (2015). A further source of spin-orbit coupling in two-dimensional structures is asymmetric interfaces (Fabian *et al.*, 2007); such contributions will not be considered in the following.

We note that the Rashba term (8) can somewhat naively be obtained from the general expression (1) by inserting a linear potential along the z axis. This approach, however, leads to values for α being several orders smaller than those inferred from experiments, and a realistic description has to take into account the influence of other bands in addition to the conduction band (Darnhofer and Rössler, 1993; de Andrada e Silva, La Rocca, and Bassani, 1997; Winkler, 2003; Fabian *et al.*, 2007; Wu, Jiang, and Weng, 2010). This procedure is effectively similar to the Foldy-Wouthuysen transformation used in relativistic quantum mechanics to reduce the full Dirac equation for four-component spinors to an effective description of the "conduction band" comprised of solutions of positive energy (Bjorken and Drell, 1965). Here the perturbative treatment of the negative-energy states ("valence band") leads to the spin-orbit coupling term (1), apart from other relativistic corrections.

B. Persistent spin helix: Basic theory

Let us first consider quantum wells grown in the [001] direction. As a result of a large body of experimental as well as theoretical work (Fabian *et al.*, 2007; Wu, Jiang, and Weng, 2010), both the parameters β and α lie in the ballpark of about $1.0\cdots 100$ meV Å for typical materials and growth geometries. In particular, the Rashba parameter can be tuned to be equal in magnitude to the Dresselhaus coefficient $\alpha = \pm\beta$. As we see shortly, this situation gives rise to a prime example of a persistent spin texture in a semiconductor nanostructure.

Let us consider a Hamiltonian consisting of the usual quadratic kinetic energy characterized by a band mass m, the Rashba term (8), and the linear Dresselhaus term (5),

$$\mathcal{H} = \frac{\hbar^2k^2}{2m} + \mathcal{H}_R + \overline{\mathcal{H}}_D^{001}, \tag{9}$$

leading to the two dispersion branches

$$\varepsilon_\pm(\vec{k}) = \frac{\hbar^2k^2}{2m} \pm k\sqrt{\alpha^2+\beta^2+2\alpha\beta\sin(2\varphi)}, \tag{10}$$

which are illustrated in Fig. 3 for different typical parameters. As seen from the figure and Eq. (10), the dispersion is clearly

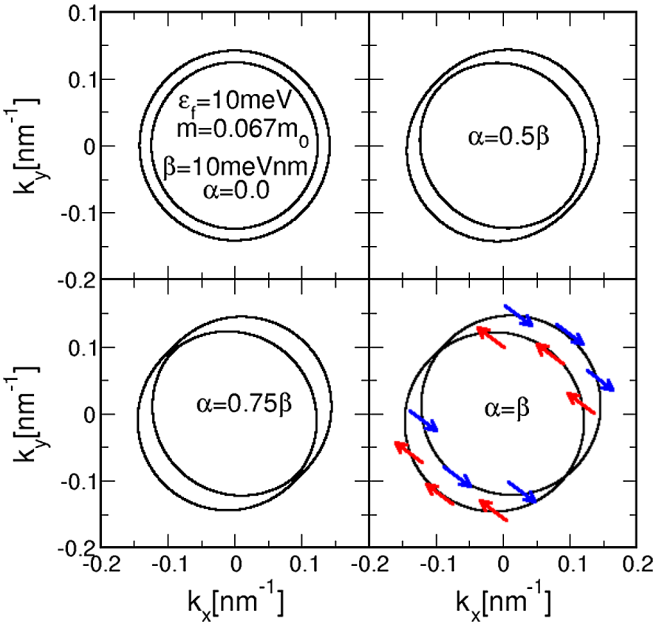

FIG. 3. Fermi contours for an electron system with band mass $m = 0.067m_0$ (corresponding to GaAs), a typical Fermi energy of $\varepsilon_f = 10$ meV, and a Dresselhaus parameter of $\beta = 10$ meV nm. With a growing Rashba parameter the energy dispersion becomes increasingly anisotropic. For the case $\alpha = \beta$ (bottom right) the spin directions being independent of wave vector are indicated. Adapted from Schliemann and Loss, 2003.

anisotropic for $\alpha \neq 0 \neq \beta$. Remarkably, this anisotropy in the dispersion relation does not lead to an anisotropy of the linear electrical bulk conductivity (Trushin and Schliemann, 2007a; Chalaev and Loss, 2008, 2009), despite an earlier statement in the literature (Schliemann and Loss, 2003).

The case $\alpha = \pm\beta$ shown in the lower right panel of Fig. 3 is particular (Schliemann, Egues, and Loss, 2003): Here the Hamiltonian (9) can be formulated as

$$\mathcal{H} = \frac{\hbar^2}{2m}[k^2 + 2(\vec{k}\cdot\vec{Q})\Sigma] \tag{11}$$

with

$$\Sigma = \frac{\mp\sigma^x + \sigma^y}{\sqrt{2}}, \qquad \vec{Q} = \frac{\sqrt{2}m\alpha}{\hbar^2}(1, \pm 1), \tag{12}$$

such that the spin operator Σ is a conserved quantity,

$$[\mathcal{H}, \Sigma] = 0. \tag{13}$$

The energy dispersions

$$\varepsilon_\pm(\vec{k}) = \frac{\hbar^2}{2m}[k^2 \pm 2(\vec{k}\cdot\vec{Q})] \tag{14}$$

form circles whose centers are displaced from the Γ point by $\mp\vec{Q}$. Differently from Eq. (10) the double sign here refers to the spin eigenvalues determined by $\Sigma\chi_\pm = \pm\chi_\pm$, where the eigenspinors read for $\alpha = +\beta$:

$$\chi_\pm = \frac{1}{\sqrt{2}}\begin{pmatrix} 1 \\ \mp e^{-i\pi/4} \end{pmatrix}, \tag{15}$$

and for $\alpha = -\beta$ the lower spin component acquires an additional factor of $(-i)$. In particular, the spin state is independent of the wave vector, i.e., spin and orbital degrees of freedom are disentangled, and the Kramers degeneracy enforced by time reversal symmetry is manifested as

$$\varepsilon_+(\vec{k} - \vec{Q}) = \varepsilon_-(\vec{k} + \vec{Q}). \tag{16}$$

The conservation of the spin component Σ expressed in Eq. (13) remains intact if a spin-independent single-particle potential or spin-independent interaction among the electrons is added to the Hamiltonian. In such a case the single-particle wave vector $\vec{k}$ will in general not be conserved any more and is to be replaced by a proper momentum operator $\vec{k} \mapsto -i\nabla$. For example, adding an arbitrary scalar potential $V(\vec{r})$ to the Hamiltonian (11) and inserting the ansatz

$$\psi_\pm(\vec{r}) = e^{-i\vec{Q}\cdot\vec{r}\Sigma}\chi_\pm\phi(\vec{r}) = e^{\mp i\vec{Q}\cdot\vec{r}}\chi_\pm\phi(\vec{r}) \tag{17}$$

into $\mathcal{H}\psi_\pm = \varepsilon\psi_\pm$ leads to the spin-independent Schrödinger equation

$$\left(-\frac{\hbar^2}{2m}\nabla^2 + V(\vec{r})\right)\phi(\vec{r}) = \left(\varepsilon + \frac{2m\alpha^2}{\hbar^2}\right)\phi(\vec{r}), \tag{18}$$

where the energy is shifted by $\hbar^2Q^2/(2m) = 2m\alpha^2/\hbar^2$. An analogous many-particle Schrödinger equation is obtained when adding to Eq. (11) an arbitrary spin-independent interaction among particles; here the spin component Σ of each electron is separately conserved.

Moreover, comparing the spin state of a general wave function composed of the states (17) at given energy,

$$\begin{aligned}\psi(\vec{r}) &= \nu_+\psi_+(\vec{r}) + \nu_-\psi_-(\vec{r}) \\ &= (\nu_+e^{-i\vec{Q}\cdot\vec{r}\Sigma}\chi_+ + \nu_-e^{-i\vec{Q}\cdot\vec{r}\Sigma}\chi_-)\phi(\vec{r})\end{aligned} \tag{19}$$

at two arbitrary locations, say $\vec{r} = 0$ and $\vec{r} = \vec{a}$, we see that the spin state of $\psi(\vec{a})$ emerges from $\psi(0)$ by applying the operator $\exp(-i\vec{Q}\cdot\vec{a}\Sigma)$. This is a *controlled rotation* being independent of any further detail of the system encoded in the single-particle potential or the interaction. As the rotation operator is also independent of energy, this observation also holds for arbitrary linear combinations of states of different energy. Thus, under these very general circumstances, the electron spin undergoes a controlled rotation as a function of position, a phenomenon later called the *persistent spin helix* (Bernevig, Orenstein, and Zhang, 2006).

The angle of the controlled rotation is $2\vec{Q}\cdot\vec{a}$ and naturally depends on the distance $\vec{a}$, while the rotation axis in spin space is defined by the conserved operator Σ and given by $(\mp 1, 1, 0)$, depending on $\alpha = \pm\beta$. As a consequence, the spin component in this direction is constant as a function of both position and time leading to an *infinite spin lifetime* as measured by the expectation value of Σ. The latter feature is of

course just a general property of any conserved operator within an equilibrium state.

Prior to the work by Schliemann, Egues, and Loss (2003), others also reported peculiarities of the system (9) at $\alpha = \beta$ although not relating their observations to the existence of a new conserved quantity. Kiselev and Kim (2000b) studied an effective spin model of the type (9) where the momentum $\vec{p} = m\dot{\vec{r}}$ is a classical quantity (also neglecting the difference between canonical and kinetic momenta due to spin-orbit coupling) whose time dependence is generated by a Markov chain modeling independent elastic scattering events. Here for general Rashba and Dresselhaus parameters, the spin is rapidly randomized via the Dyakonov-Perel spin relaxation mechanism (Dyakonov and Perel, 1972). For $\alpha = \pm\beta$ the time ordering $\mathcal{T}$ in the time evolution operator $\mathcal{U}(t) = \mathcal{T}\exp[-i\int_0^t dt'\mathcal{H}(p(t'))/\hbar]$ becomes trivial such that it takes, up to a global phase factor, the form of the global spin rotation operator (Schliemann, Egues, and Loss, 2003),

$$\mathcal{U}(t) = \exp\left(-i\vec{Q}\cdot\vec{a}(t)\Sigma\right) \tag{20}$$

with $\vec{a}(t) = \vec{r}(t) - r(0)$. In particular, Kiselev and Kim (2000b) observed a diverging spin lifetime for expectation values of Σ; a similar conclusion was reached by Cartoixa, Ting, and Chang (2003), slightly subsequent to the work by Schliemann, Egues, and Loss (2003). The suppressed relaxation of appropriate spin components was also found earlier by Averkiev and Golub (1999).

In another theoretical investigation Pikus and Pikus (1995) concluded that contributions of Rashba and Dresselhaus spin-orbit coupling to the electrical conductivity cancel each other at $\alpha = \beta$ (albeit both terms were predicted there to contribute additively to spin relaxation, in contrast to the results demonstrated earlier). Tarasenko and Averkiev (2002) studied the combined influence of Rashba and Dresselhaus contributions to the beating patterns of Shubnikov–de Haas oscillations and predicted an effective cancellation of the terms at $\alpha = \beta$. Finally, the very fact that Rashba and Dresselhaus spin-orbit coupling can nontrivially interfere rather than simply add up was already observed theoretically by Knap *et al.* (1996) within investigations of weak localization phenomena.

Writing the Hamiltonian (11) in the form

$$\mathcal{H} = \frac{1}{2m}\left(\vec{p} + \hbar\vec{Q}\Sigma\right)^2 - \frac{\hbar^2\vec{Q}^2}{2m} \tag{21}$$

suggests to interpret the operator $\exp(-i\vec{Q}\cdot\vec{r}\Sigma)$ occurring in Eqs. (17) and (19) as a gauge transformation and $\vec{p}$ as a gauge-dependent canonical momentum (Chen and Chang, 2008; Tokatly and Sherman, 2010). Moreover, since the Hermitian 2×2 matrix Σ generates SU(2) transformations, the question arises whether the Hamiltonian (21) admits further symmetries furnishing a full representation of the Lie algebra su(2). Following Bernevig, Orenstein, and Zhang (2006) this can be achieved by writing the Hamiltonian in second-quantized form,

$$\mathcal{H} = \sum_{\vec{k}\eta}\frac{\hbar^2}{2m}\left(k^2 + 2\eta\vec{Q}\cdot\vec{k}\right)c^+_{\vec{k}\eta}c_{\vec{k}\eta} \tag{22}$$

along with

$$T^3 = \frac{\Sigma}{2} = \sum_{\vec{k}\eta}\frac{\eta}{2}c^+_{\vec{k}\eta}c_{\vec{k}\eta}, \tag{23}$$

where $c^+_{\vec{k}\eta}$ ($c_{\vec{k}\eta}$) creates (annihilates) an electron with wave vector $\vec{k}$ and spin state χ_η, $\eta = \pm$. Defining now

$$T^+_{\vec{Q}} = \sum_{\vec{k}} c^+_{(\vec{k}-\vec{Q})+}c_{(\vec{k}+\vec{Q})-} \tag{24}$$

and its adjoint $T^-_{\vec{Q}} = (T^+_{\vec{Q}})^+$ one easily verifies that the latter two operators together with T^3 fulfill the su(2) commutation relations,

$$[T^+_{\vec{Q}}, T^-_{\vec{Q}}] = 2T^3, \qquad [T^3, T^\pm_{\vec{Q}}] = \pm T^\pm_{\vec{Q}} \tag{25}$$

and commute, just as T^3, with the Hamiltonian,

$$[\mathcal{H}, T^\pm_{\vec{Q}}] = 0. \tag{26}$$

Moreover, since $T^\pm_{\vec{Q}}$ also commutes with any Fourier component of the density $\rho_{\vec{q}} = \sum_{\vec{k}\eta}c^+_{\vec{k}\eta}c_{(\vec{k}+\vec{q})\eta}$,

$$[\rho_{\vec{q}}, T^\pm_{\vec{Q}}] = 0, \tag{27}$$

Eq. (26) remains also valid if arbitrary spin-independent potentials or interactions are added to the Hamiltonian. We note that the su(2) commutation relation (25) as well as the property (27) holds for any vector $\vec{Q}$. The vanishing of the commutator (26), however, depends on the specific form given in Eq. (12) and the fact that the spin-independent part of the kinetic Hamiltonian (11) is quadratic in the wave vector leading to the degeneracy (16). For instance, if a term quartic in the momentum were present (still consistent with time reversal symmetry), Eq. (26) would not hold, and also a formulation (21) as the style of a gauge theory would not be possible.

Applying an in-plane magnetic field perpendicular to $\vec{Q}$ (i.e., in the direction defined by Σ) changes the Hamiltonian as

$$\mathcal{H}' = \sum_{\vec{k}\eta}\left[\frac{\hbar^2}{2m}k^2 + \eta\left(\frac{\hbar^2}{m}\vec{Q}\cdot\vec{k} + \frac{\Delta}{2}\right)\right]c^+_{\vec{k}\eta}c_{\vec{k}\eta} \tag{28}$$

with Δ being the Zeeman gap. This alteration breaks the SU(2) symmetry down to U(1) as the Hamiltonian of course still commutes with Σ but not with $T^\pm_{\vec{Q}'}$ for any choice of $\vec{Q}'$ since

$$[\mathcal{H}', T^\pm_{\vec{Q}'}] = \sum_{\vec{k}}\left(\frac{2\hbar^2}{m}\vec{k}\cdot(\vec{Q}-\vec{Q}') + \Delta\right)c^+_{(\vec{k}-\vec{Q})+}c_{(\vec{k}+\vec{Q})-}. \tag{29}$$

The operators $T^\pm_{\vec{Q}}$ are defined with respect to the explicit spinors (15). In terms of the usual spin density $\vec{S}_{\vec{q}} = (1/2)\sum_{\vec{k}}\sum_{\mu\nu}c^+_{\vec{k}\mu}\vec{\sigma}_{\mu\nu}c_{(\vec{k}+\vec{q})\nu}$ defined with respect to the original

spin coordinates underlying the Hamiltonian (9) they can be expressed as

$$T^{\pm}_{\vec{Q}} = S^{z}_{\pm 2\vec{Q}} \pm i\frac{\vec{Q}}{|\vec{Q}|}\cdot\vec{S}_{\pm 2\vec{Q}}, \tag{30}$$

i.e., they describe the spin components perpendicular to the quantization axis defined by $\Sigma = 2T^3$. Defining the Hermitian combinations $T^1 = (T^+ + T^-)/2$, $T^2 = (T^+ - T^-)/(2i)$, we obtain an su(2)-valued vector $\vec{T}$ of observables commuting with the Hamiltonian. Thus, the expectation value $\langle\vec{T}\rangle$ within any pure state is constant in time. Regarding mixed states, a sufficient condition for a constant expectation value is to demand that the density operator is only a function of the Hamiltonian itself, $\rho = \rho(\mathcal{H})$, as typical for equilibrium situations. However, such a density matrix is also invariant under arbitrary spin rotations generated by $\vec{T}$ such that, as usual for rotationally invariant magnetic systems, $\langle\vec{T}\rangle$ vanishes. In other words, a finite expectation value $\langle\vec{T}\rangle$ is the consequence of a nonequilibrium state or the result of spontaneous symmetry breaking. The latter should of course not be expected in a two-dimensional system.

For quantum wells with growth direction [110] the Dresselhaus term (6) commutes with σ^z. Thus, the analog of the Hamiltonian (9) allows for a conserved spin quantity if the Rashba spin-orbit coupling is absent. In this case the Hamiltonian can again, neglecting the cubic third-harmonic contribution to the Dresselhaus coupling, be formulated as in Eq. (11) with

$$\Sigma = \sigma^z, \qquad \vec{Q} = \frac{m\beta}{2\hbar^2}(0,1). \tag{31}$$

With these replacements, analogous properties as obtained for [001] quantum wells at $\alpha = \pm\beta$ follow. In particular, an SU(2) symmetry as described in Eqs. (22)–(27) also occurs here which is in the present case broken down to U(1) by applying a magnetic field along the growth direction [cf. Eqs. (28) and (29)].

Finally, for quantum wells grown into the [111] direction the linear part of the Dresselhaus coupling (7) and the Rashba term (8) have the identical functional form. Here a conserved quantity can be realized only if these two contributions exactly cancel each other (Cartoixa, Ting, and Chang, 2005a, 2005b; Vurgaftman and Meyer, 2005).

Moreover, in a very recent work Kammermeier, Wenk, and Schliemann (2016) extended the previous considerations to more general growth directions. Specifically it was demonstrated that a conserved spin operator exists for appropriately tuned Rashba coupling, if and only if two Miller indices of the growth direction agree in modulus. Fully analogously to the cases discussed earlier, these conserved spin components are extended to an su(2) algebra of operators commuting with the Hamiltonian.

C. Spin diffusion equations

Let us concentrate again on [001] quantum wells. As seen before, for balanced contributions to spin-orbit coupling $\alpha = \pm\beta$ an electron spin undergoes a perfectly controlled rotation provided the locations of injection and detection of the electron are sufficiently defined, for instance in terms of quantum point contacts (Schliemann, Egues, and Loss, 2003). This, however, is a rather special situation in experiments. In order to treat more general scenarios it is useful to study the expectation value of the local spin density,

$$\vec{s}(\vec{r},t) = \left\langle \sum_a \frac{\hbar}{2}\vec{\sigma}_a \delta(\vec{r} - \vec{r}_a(t)) \right\rangle, \tag{32}$$

where a labels the electrons, and the average $\langle\cdot\rangle$ is to be taken over the given (in general nonequilibrium) state in the presence of disorder potentials and/or interactions among the charge carriers. Moreover, we also include the cubic third-harmonic correction to the Dresselhaus term (3) proportional to β_3. Effective semiclassical diffusion equations for $\vec{s}(\vec{r},t)$ can be derived via quantum kinetic equations rooted in the Keldysh formalism (Mishchenko, Shytov, and Halperin, 2004). Working in Fourier space at small frequencies and wave vectors, and evaluating the arising parameters within the zero-temperature ground state, one obtains in the regime of weak spin-orbit coupling (Bernevig, Orenstein, and Zhang, 2006; Stanescu and Galitski, 2007; Liu and Sinova, 2012; Salis *et al.*, 2014)

$$(-i\omega + Dq^2 + D_{\rm so}) \begin{pmatrix} \overline{s}^1(\vec{q},\omega) \\ \overline{s}^2(\vec{q},\omega) \\ \overline{s}^3(\vec{q},\omega) \end{pmatrix} = 0 \tag{33}$$

with

$$D_{\rm so} = 2k_f^2\tau \begin{pmatrix} \left[(\alpha+\beta)^2 + \beta_3^2\right]/\hbar^2 & 0 & i(\alpha+\beta)\overline{q}_1/m \\ 0 & \left[(\alpha-\beta)^2 + \beta_3^2\right]/\hbar^2 & i(\alpha-\beta)\overline{q}_2/m \\ -i(\alpha+\beta)\overline{q}_1/m & -i(\alpha-\beta)\overline{q}_2/m & 2(\alpha^2+\beta^2+\beta_3^2)/\hbar^2 \end{pmatrix}. \tag{34}$$

In Eq. (33) we used a rotated coordinate system in the plane of the quantum well $\overline{s}^{1,2} = (\pm s^x + s^y)/\sqrt{2}$, $\overline{s}^3 = s^z$, and likewise for the wave vector $\vec{q}$, such that the new axes are along [110] and $[1\overline{1}0]$. $D = v_f^2\tau/2$ is the usual diffusion constant given in terms of the momentum relaxation time τ and the Fermi velocity $v_f = \hbar k_f/m$ for an effective Fermi wave vector k_f (again neglecting spin splitting). Equation (33) is valid in the regime of weak spin-orbit

interaction $(\alpha,\beta,\beta_3)k_f\tau/\hbar \ll 1$. Diffusion equations similar to Eqs. (33) and (34) have, for various types of spin-orbit coupling and ingredients to the many-body physics, also been derived using different theoretical techniques (Kalevich, Korenev, and Merkulov, 1994; Burkov, Núñez, and MacDonald, 2004; Raimondi *et al.*, 2006; Schwab *et al.*, 2006; Kleinert and Bryksin, 2007, 2009; Bernevig and Hu, 2008; Wenk and Kettemann, 2010; Yang, Orenstein, and Lee, 2010; Lüffe, Kailasvuori, and Nunner, 2011; Lüffe, Danon, and Nunner, 2013).

All the effects of spin-orbit interaction in the diffusion equation (33) are encoded in the matrix (34). As expected, this equation also reflects the symmetry properties arising for balanced Rashba and Dresselhaus coupling as analyzed in Sec. II.B: At, say, $\alpha=\beta$ the equation for $\overline{s}^2$ decouples from the remaining system and reads in real space

$$(\partial_t - D\nabla^2 + 1/T_1)\overline{s}^2(\vec{r},t) \tag{35}$$

with $1/T_1 = 2k_f^2\tau(\beta_3/\hbar)^2$ and the general solution

$$\overline{s}^2(\vec{r},t) = \frac{e^{-t/T_1}}{(2\pi)^2}\int d^2q e^{-Dq^2t}\overline{s}^2(\vec{q},t=0)e^{i\vec{q}\cdot\vec{r}}. \tag{36}$$

Equation (36) describes the diffusion of an initial spin polarization, accompanied by its decay on the time scale T_1 which, as suggested by the notation, is aptly referred to as a decoherence time. Without the cubic third-harmonic correction to the Dresselhaus term $\beta_3=0$, no decay occurs, and all the dynamics is due to the diffusive motion of electrons with fixed spin governed by the particle (or charge) diffusion constant D. We note that the spin density can be changed by either moving the particles or altering their spin. Because of the latter mechanism, the spin density does, differently from the charge density, fulfill a continuity equation with additional source terms (Erlingsson, Schliemann, and Loss, 2005). The infinite spin relaxation time occurring at $\alpha=\pm\beta$ and $\beta_3 \propto 1/T_1 = 0$ was confirmed by several on the basis of Monte Carlo simulations treating the orbital carrier dynamics classically (Kiselev and Kim, 2000b; Ohno and Yoh, 2007, 2008; Liu *et al.*, 2010); for an analytical approach see also Lyubinskiy and Kachorovskii (2006) and Wenk and Kettemann (2011).

The two other solutions to Eq. (33) are for $\alpha=\beta$ and $\beta_3=0$ characterized by the frequencies

$$i\omega_\pm(\vec{q}) = Dq^2 \pm 8k_f^2\tau[(\alpha/\hbar)^2 + (\alpha\overline{q}_1/m)^2]. \tag{37}$$

Now for $\vec{q}$ being twice the "shift vector" $\pm\vec{Q}$ as occurring in Eqs. (12) and (16), i.e., $\overline{q}_1 = \pm 2|\vec{Q}|$, $\overline{q}_2=0$, we have $\omega_-=0$ (Bernevig, Orenstein, and Zhang, 2006). This static solution describes the persistent spin helix and reads in real space

$$\begin{pmatrix}\overline{s}^1(\vec{r})\\ \overline{s}^3(\vec{r})\end{pmatrix} = A\begin{pmatrix}\cos(2\vec{Q}\,\vec{r}+\phi)\\ -\sin(2\vec{Q}\,\vec{r}+\phi)\end{pmatrix} \tag{38}$$

with two real constants A and ϕ. Naturally, the angular argument $2\vec{Q}\cdot\vec{r}$ of the spin rotation around the $[1\bar{1}0]$ direction occurring here is the same as (for $\vec{r}=\vec{a}$) in the effective evolution operator (20): The spatial dependence of the spin density (38) precisely mimics the rotation of the spin of an electron moving along the direction of $\vec{Q}$. Figure 4 shows a sketch of the helical spin structure described by Eq. (38).

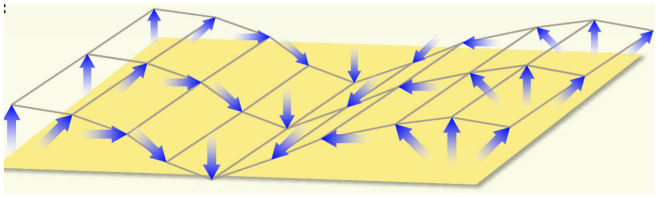

FIG. 4. Schematic of the persistent spin helix occurring in a [001] quantum well for spin-orbit coupling tuned to $\alpha=\beta$ according to Eq. (38). The shift vector $\vec{Q}$ defines the pitch of the helix and points along the lateral direction. The spin density component in the longitudinal direction vanishes, $\overline{s}^2=0$. Adapted from Fabian, 2009.

D. [001] Quantum wells: Experiments and simulations

We now review experimental work investigating the high-symmetry situation $\alpha=\pm\beta$ in [001] quantum wells, along with numerical simulations and pertinent theoretical approaches.

1. Optical techniques

The stability of periodic spin structures in GaAs quantum wells close to the regime $\alpha\approx\beta$ was experimentally studied by Koralek *et al.* (2009) using the technique of transient spin-grating spectroscopy. Here a periodic spin pattern with defined wave vector $\vec{q}$ is created via optical orientation by two noncollinear laser beams, and its time evolution is then monitored by diffraction of a time-delayed probe pulse. The initial spin density structure is a superposition of two helices with the same $\vec{q}\|[110]$ but different senses of rotation, only one of which matches the one encoded in the static solution (38). Accordingly, Koralek *et al.* (2009) observed that the initial spin polarization decays, to about equal weights, on two very distinct time scales as shown in Fig. 5: A short-lived part where the lifetime shows a maximum at $q=0$ and slowly decreases with growing wave number, and a fraction with clearly enhanced lifetime attaining a pronounced maximum at $q\approx 10^6$ m^{-1}. The latter should be interpreted as a persistent spin helix (38) with $q=2Q=4m\alpha/\hbar^2$ corresponding to a Rashba parameter of $\alpha\approx 3$ meV Å. The fact that these measurements indeed explore the regime $\alpha\approx\beta$ was further established by varying the Rashba and Dresselhaus parameter (see lower panels of Fig. 5): The first was achieved by studying samples with altered relative concentration of the remote dopants on both sides of the quantum well at fixed total density of dopants, while in the latter case samples of different well width were compared.

In a related experimental study Yang *et al.* (2012) investigated, also using transient spin-grating spectroscopy, the drift dynamics of spin helices in the presence of an electric field directed in the plane of a *symmetric* quantum well with a

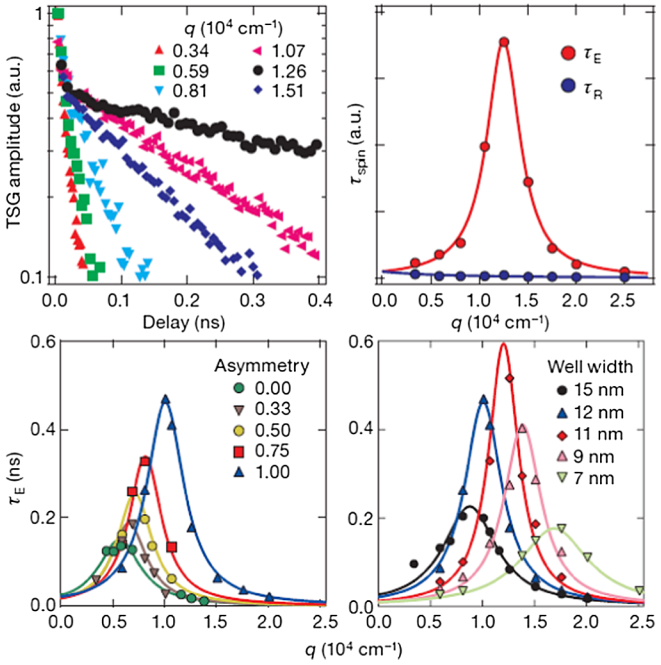

FIG. 5. Upper left panel: Decay curves of spin gratings obtained by Koralek *et al.* (2009) for different wave numbers q of the initially modulated spin density. The data show decay on two distinct time scales. Upper right panel: Lifetimes of the spin helices with enhanced (τ_E) and reduced (τ_R) stability. The former one corresponds to the spin density configuration (38) with a maximum lifetime at $q = 2Q$. Lower panels: Lifetime of the spin helix configuration as a function of the wave number for different doping asymmetry (varying the Rashba coupling, left) and well width (varying the Dresselhaus term, right). Adapted from Koralek *et al.*, 2009.

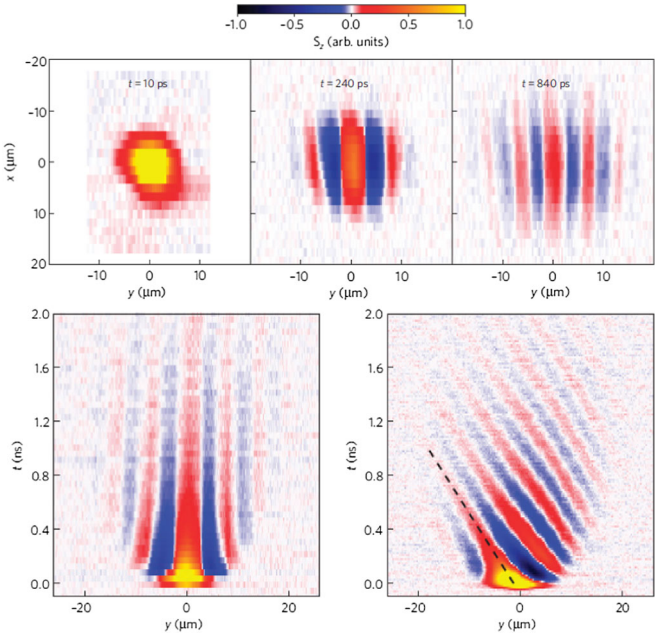

FIG. 6. Kerr rotation data obtained by Walser *et al.* (2012). The detection method is sensitive to the out-of-plane component s^z of the spin density. Upper panels: Time evolution of the persistent spin helix from an initial local spin polarization along the growth direction (left) generated by a pump laser. Here the x and y directions point along $[1\bar{1}0]$ and [110], respectively, and the detection method is sensitive only to the out-of-plane component $s^z(\vec{r}, t)$ of the spin density shown. Lower panels: Time evolution of the spin density in zero magnetic field (left) and in an in-plane field of $B = -1$ T along $[1\bar{1}0]$ rotating the in-plane spin components into the growth direction. Adapted from Walser *et al.*, 2012.

vanishing Rashba but finite Dresselhaus parameter. These spin helices have of course *per se* a finite lifetime.

The formation of a persistent spin helix was directly observed by Walser *et al.* (2012) using spatially and temporally resolved Kerr microscopy. They monitored the time evolution of a local spin polarization along the growth (or z) direction produced by a focused pump laser. The upper panels of Fig. 6 show the spreading of this initial wave packet by diffusion: The z component of the spin density evolves, due to the combined Rashba and Dresselhaus spin-orbit coupling near $\alpha = +\beta$, into an oscillatory pattern along the [110] direction, consistent with numerical simulations by Liu *et al.* (2006, 2009). As expected, the spin density pattern is constant in the orthogonal $[1\bar{1}0]$ direction. Similar to the measurements by Koralek *et al.* (2009), the detection technique is sensitive only to the z component of the spin density. Applying an external magnetic field in the $[1\bar{1}0]$ direction coupling to the conserved spin component Σ rotates the in-plane component of the helix into the growth direction and enables its detection (lower panels of Fig. 6). We note that, as seen in Eqs. (22) and (29), introducing such an external field breaks the SU(2) symmetry at $\alpha = \beta$. Thus, the work by Walser *et al.* (2012) is an experimental demonstration that the stability of the persistent spin helix does not depend on the full SU(2) symmetry but the existence of the single conserved spin component Σ suffices.

The investigations by Walser *et al.* (2012) were performed in a [001]-grown GaAs quantum well with the Rashba parameter fixed by asymmetric doping. Ishihara, Ohno, and Ohno (2014a) conducted a similar imaging study on a sample where the Rashba parameter was varied by a gate voltage close to $\alpha = -\beta$. In a companion study they used Kerr imaging to map out the spin dynamics in quantum wires lithographically defined in the quantum well along the [110] and $[1\bar{1}0]$ directions (Ishihara, Ohno, and Ohno, 2014b). In accordance with Eqs. (11) and (12) (again for $\alpha = -\beta$), the spin-orbit coupling was found to be strongly suppressed in the former case (where $\vec{k} \perp \vec{Q}$), while in the latter case a spin helix was formed. Similar results on spin dephasing time scales for quantum wires in GaAs wells close to $\alpha = -\beta$ were reported by Denega *et al.* (2010).

Salis *et al.* (2014) combined the experimental techniques of Walser *et al.* (2012) with theoretical simulations to study the formation of a spin helix, again following a local optical spin excitation, under imperfect conditions. Specifically, they considered a finite imbalance $|\alpha| - \beta \neq 0$, a substantial third-harmonic cubic correction to the Dresselhaus term, and lateral confinement within the quantum well. The experimental results obtained again for GaAs samples were found to agree well with the theoretical modeling. Only a short while later the same collaboration (Altmann *et al.*, 2014) investigated, in a similar experimental setup, the spin helix lifetime

near $\alpha = \beta$ in quantum wires etched along the direction $[110] \| \vec{Q}$ in quantum wells originating from the same wafer as used before (Walser *et al.*, 2012). By fitting their data to a spin diffusion model (Salis *et al.*, 2014) (cf. Sec. II.C) they concluded that the observed enhanced stability of the helix is mainly due to the geometrical confinement while the intrinsic lifetime is rather unaffected and still determined essentially by the cubic third-harmonic contribution to the Dresselhaus term.

Schönhuber *et al.* (2014) investigated via inelastic light scattering intrasubband spin excitations in a GaAs quantum well close to $\alpha = \beta$ produced again from the same wafer as used by Walser *et al.* (2012). For momentum transfer along the $\vec{Q} \| [110]$ direction a substantial spin splitting is found, while this quantity is clearly suppressed in the opposite direction, in accordance with Eqs. (11) and (12) and the findings by Ishihara, Ohno, and Ohno (2014b) (working at $\alpha = -\beta$). The spin-orbit parameters extracted from the measurements are consistent with the results by Walser *et al.* (2012).

Most recently, two studies extended the work of Yang *et al.* (2012) mentioned previously on spin helix drift in quantum wells now close to $\alpha = \pm\beta$. Kunihashi *et al.* (2016) investigated drift spin transport via Kerr imaging in a four terminal geometry of Ohmic contacts covered by a semitransparent Au gate electrode. The latter varied the Rashba coupling while voltages applied to the contacts created drift transport of optically injected spin-polarized electrons. Wells of two widths ($L = 15$ and 25 nm) were studied with the wider one being close to $\alpha = -\beta$, and a clearly enhanced spatial coherence of the drifting spin pattern was observed here. They also demonstrated the modulation of the electron transport path upon applying time-dependent drift voltages. Altmann *et al.* (2016) used samples of the same structure as Walser *et al.* (2012) to perform a Kerr imaging study concentrating on the situation where the diffusive current of the optically injected spin density is compensated by the drift current. Here a spin precession is found with a frequency proportional to the drift velocity. Using an appropriate model for the carrier distribution function (being anisotropic as a function of wave vector) they explained this effect with properties of the cubic Dresselhaus term.

2. Transport measurements

Kohda *et al.* (2012) investigated the quantum corrections to the magnetoconductance in InGaAs quantum wells with spin-orbit coupling close to $\alpha = \beta$. The spin-orbit interaction combined with scattering on imperfections generically randomizes the spin leading to weak antilocalization signaled by a negative magnetoconductance (Knap *et al.*, 1996; Schäpers *et al.*, 2006; Wirthmann *et al.*, 2006; Kettemann, 2007). For Rashba and linear Dresselhaus spin-orbit interactions at $\alpha = \pm\beta$, however, spins are left unaltered along closed trajectories which should give rise to weak localization, i.e., a positive magnetoconductance. Kohda *et al.* (2012) applied the magnetic field perpendicular to the quantum well and used a gate voltage across it to vary the Rashba parameter α. As shown in Fig. 7, in a comparatively narrow well of width $L = 4$ nm they found a transition from weak antilocalization to weak localization and back when driving the gate voltage through an appropriate critical value. In a sample with a larger well width of $L = 7$ nm and therefore smaller Dresselhaus parameter β no such behavior was observed, i.e., in the latter system β and the range of α seem to be too different to match each other. The experimental results are corroborated by numerical simulations which conclude that the weak localization signal persists even if the cubic third-harmonic term in Eq. (3) is included, but its location in parameter space is shifted away from $\alpha = \beta$.

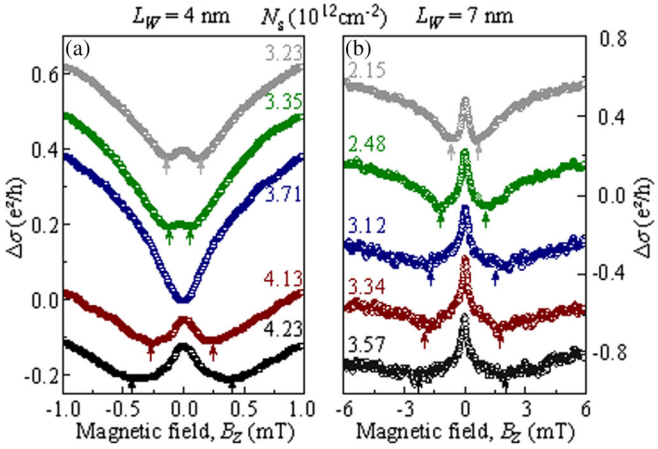

FIG. 7. Measured magnetoconductance for different gate voltages in two quantum wells differing in width. In the narrower well (left) a transition from weak antilocalization to weak localization and back occurs. From Kohda *et al.*, 2012.

The fact that the $L = 4$ nm sample actually has spin-orbit coupling parameters close to $\alpha = \beta$ was also established by Kohda *et al.* (2012) in an independent experiment using the spin-galvanic effect. This phenomenon amounts to an electric current in response to an in-plane spin polarization, and its directional dependence is highly sensitive to the ratio α/β (Ganichev *et al.*, 2004; Trushin and Schliemann, 2007a; Ganichev and Golub, 2014), which was indeed found to be close to unity.

Dettwiler *et al.* (2014) extended the investigations by Kohda *et al.* (2012) using GaAs quantum wells varying in width from $L = 8$ to 13 nm. Employing a combination of top and back gates the Rashba parameter α and the carrier density n could be tuned independently. The point $\alpha = \beta$ was again determined by monitoring the transition from weak antilocalization to weak localization and back. To obtain a consistent data analysis it was necessary to take into account the cubic correction (being proportional to n) to the Dresselhaus parameter β. As a result, Dettwiler *et al.* (2014) demonstrated control over spin-orbit coupling parameters and carrier density while preserving the condition $\alpha = \beta$. At quite high densities such as $n = 9 \times 10^{11}$ cm^{-2} no transition between weak antilocalization and localization was found which should be ascribed to the third-harmonic correction to the Dresselhaus term that also increases with density.

Magnetoconductance studies in quantum wires in the directions [100], [110], and $[1\bar{1}0]$ of an [001] InGaAs quantum well were performed by Sasaki *et al.* (2014) building upon theoretical work by Scheid *et al.* (2008). To reduce fluctuation effects they used arrays of wires which were arranged in the same sample thus enabling simultaneous measurements.

The Rashba coupling was varied by a top gate, and the magnetic field lay in the plane of the well leading in combination with the spin-orbit coupling to a strong anisotropy of the magnetoconductance, which additionally depends on the direction of the wire. In a one-dimensional quantum wire spin randomization due to momentum scattering (Dyakonov-Perel mechanism) is quenched since the effective wave-vector-dependent field provided by the spin-orbit interaction is unidirectional. This phenomenon is discussed in more detail in Sec. II.F.4. An in-plane magnetic field noncollinear with the spin-orbit field changes this situation and leads to spin randomization favoring weak antilocalization. Thus, in accordance with the numerical simulation done by the authors, the weak localization signal in the conductance is maximal if the applied field is collinear with the field provided by the spin-orbit coupling. With the direction of the wave vector defined by the quantum wire, the latter observation provides a means to determine the ratio α/β. In particular, for $\alpha/\beta = 1$ no anisotropy of the magnetoconductance is observed for transport in the $[1\bar{1}0]$ direction since here we have $\vec{k} \perp \vec{Q}$ [cf. Eqs. (11) and (12)]. If the applied magnetic field is substantially noncollinear with the spin-orbit field, it randomizes the spin and suppresses weak localization. Assuming that this process is most efficient if both fields are of the same magnitude (as indicated by the numerics), Sasaki *et al.* (2014) also give reasonable separate estimates for α and β. For a further proposal to determine the relative strength of the Rashba and Dresselhaus coupling utilizing the high-symmetry point $|\alpha/\beta| = 1$, see Li and Chang (2010).

Most recently, Yoshizumi *et al.* (2016) demonstrated gate-controlled switching between $\alpha = \pm\beta$ in an InAlAs quantum well. The occurrence of each persistent spin helix (differing by sense of rotation) was again detected by similar magnetoconductance measurements.

3. Stability of the spin helix: Limiting factors

Several theoretical studies have identified the cubic Dresselhaus term as the main decay mechanism of the persistent spin helix (Lusakowski, Wrobel, and Dietl, 2003; Cheng and Wu, 2006; Cheng, Wu, and da Cunha Lima, 2007; Kettemann, 2007; Shen and Wu, 2009; Lüffe, Kailasvuori, and Nunner, 2011; Wenk and Kettemann, 2011; Liu and Sinova, 2012; Kurosawa *et al.*, 2015) in accordance with experiments already mentioned (Koralek *et al.*, 2009; Salis *et al.*, 2014).

Specifically, the spin-grating experiments by Koralek *et al.* (2009) found the spin lifetime τ_h of the symmetry-protected spin helix to be of the order of a few hundred picoseconds, depending significantly on temperature. The ratio of τ_h and the time scale of ordinary (spin) diffusion can be expressed as $\eta := 4DQ^2\tau_h$. This quantity is constant $\eta \approx 100$ below 50 K, while it decreases for higher temperature with a power law showing an exponent slightly larger than 2. The subsequent theoretical analysis by Liu and Sinova (2012) concluded that this temperature dependence cannot be quantitatively described by a low-order treatment of the spin-orbit interaction which is essentially restricted to the Dyakonov-Perel regime and leads to the diffusion equations (33) and (34) (given here at zero temperature). This finding is in qualitative agreement with the experimental study by Studer *et al.* (2009) on InGaAs quantum wells using time-resolved Faraday rotation. Instead the Elliot-Yafet relaxation mechanism should also be taken into account which yields expressions somewhat more involved than Eqs. (33) and (34).

Theoretical investigations by Lüffe, Kailasvuori, and Nunner (2011) and Lüffe, Danon, and Nunner (2013) led to the prediction that the spin helix lifetime can be enhanced by Coulomb repulsion (treated there within the Hartree-Fock approximation). A study of Rashba and Dresselhaus coupling and its interplay with Coulomb interaction described by the *GW* approximation was presented by Nechaev, Echenique, and Chulkov (2010).

A further possible source of decoherence of the spin helix is spatial inhomogeneities of the effective Rashba coupling (Liu *et al.*, 2006; Glazov, Sherman, and Dugaev, 2010; Bindel *et al.*, 2016).

E. Many-body signatures of the persistent spin helix

We now summarize the role of persistent spin textures in connection with the many-body physics of interacting systems. If not mentioned otherwise, we consider electrons in [001] quantum wells subjected to Coulomb repulsion and spin-orbit coupling of the Rashba and the linear Dresselhaus type.

Badalyan *et al.* (2009, 2010) evaluated the dielectric function of the two-dimensional electron gas within the random phase approximation (Lindhard formula). For $\alpha = \pm\beta$ one obtains the dielectric response of the system without spin-orbit coupling, while for general parameters a beating of the static Friedel oscillations is observed. In a subsequent work the charge density relaxation propagator, i.e., the slope of the imaginary part of the polarization function, and its analyticity properties were studied (Badalyan *et al.*, 2013).

The optical conductivity was calculated by Maytorena, Lopez-Bastidas, and Mireles (2006) and compared with the frequency dependence of the spin Hall conductivity [which vanishes in the static limit (Schliemann, 2006)]. They predicted a rich phenomenology arising from the interplay of the two spin-orbit coupling terms. In a subsequent work the analysis was extended to the optical (i.e., spatially homogeneous) spin susceptibility (Lopez-Bastidas, Maytorena, and Mireles, 2007). The optical conductivity for quantum wells with Rashba and Dresselhaus coupling was reconsidered by Li, Marsiglio, and Carbotte (2013). As a signature of the persistent spin helix, all interband transitions vanish at $\alpha = \pm\beta$. If the cubic Dresselhaus contribution is taken into account, these transitions are rendered finite but still suppressed.

Capps, Marinescu, and Manolescu (2015) studied the finite-temperature equilibrium state of an interacting electron gas at $\alpha = \pm\beta$ within the Hartree-Fock approximation and concluded the absence of any helical spin structures: a finding consistent with the fact that, as discussed in Sec. II.B, finite expectation values of the operators (23) and (24) occur only in nonequilibrium states or as the result of spontaneous symmetry breaking. Most recently, they extended their analysis to the spin Seebeck effect (Capps, Marinescu, and Manolescu, 2016).

The Ruderman-Kittel-Kasuya-Yoshida interaction between magnetic moments in the presence of spin-independent disorder was investigated by Chesi and Loss (2010). Here

the disorder-averaged susceptibility shows a twisted exchange interaction decaying exponentially with distance. Iglesias and Maytorena (2010) investigated the dynamical spin polarization, i.e., the linear response of the spin magnetization to a homogeneous in-plane electric field. They considered Rashba and Dresselhaus spin-orbit coupling in quantum wells with growth directions [001], [110], and [111].

When the electrons are confined to a quantum wire (and their interaction is neglected) the spin-orbit coupling in general leads to anticrossings of the single-particle subband dispersions except for the case $\alpha = \pm\beta$ where, due to the additional conserved quantity, crossings occur (Schliemann, Egues, and Loss, 2003). Using a Luttinger liquid description, Meng, Klinovaja, and Loss (2014) studied the renormalization of such (anti)crossings in the presence of Coulomb repulsion. This effect is especially significant near the high-symmetry point $\alpha = \pm\beta$, where the anticrossing gap vanishes with an interaction-dependent power law in the spin-orbit parameters.

F. Other growth directions and geometries

We now review, among other items, experimental studies dedicated to persistent spin structures in quantum wells of the other high-symmetry growth directions [110] and [111]. A very recent prediction of analogous phenomena in systems of more general growth direction was already mentioned (Kammermeier, Wenk, and Schliemann, 2016). For a summary of experimental work on spin-orbit coupling in such systems (not specifically addressing spin helices) see Ganichev and Golub (2014).

1. [110] quantum wells

As seen in Sec. II.B, for quantum wells grown in the [110] direction a conserved spin component along with an SU(2) symmetry involving an appropriate wave vector transfer occurs in the absence of Rashba coupling. Relying on optical techniques several groups reported on clearly enhanced spin dephasing times compared to those observed in quantum wells of other growth directions (Ohno *et al.*, 1999; Couto *et al.*, 2007; Schreiber *et al.*, 2007a, 2007b; Bel'kov *et al.*, 2008; Müller *et al.*, 2008; Völkl *et al.*, 2011, 2014). Moreover, spin dephasing is found to be strongly anisotropic depending on whether the spin polarization lies in the plane of the quantum well or along the growth direction where the longest lifetimes occur (Döhrmann *et al.*, 2004; Griesbeck *et al.*, 2012). These observations are of course in agreement with the structure of the Dresselhaus spin-orbit coupling, and the remaining spin decay can be attributed to residual Rashba coupling (Tarasenko, 2009; Glazov, Semina, and Sherman, 2010; Poshakinskiy and Tarasenko, 2013) and/or hole-mediated processes (Völkl *et al.*, 2011).

Experiments directed explicitly toward helical spin structures were performed by Chen *et al.* (2014) who studied [110]-grown GaAs quantum wells using time-resolved Kerr microscopy. To generate a finite net spin-orbit field averaged over the the Fermi contour, the Fermi disk was shifted from its equilibrium position by applying a dc current of up to 200 μA. The direction of the current defines the direction of the effective wave vector to be inserted into the Dresselhaus Hamiltonian (6). Additionally a magnetic field of the order of a few hundred millitesla (mT) was applied. By comparing data obtained for different directions of the magnetic field, they were able to extract the energy contribution due to spin-orbit interaction. For a current along the $[1\bar{1}0]$ (or y) direction this quantity is proportional to the current strength, while for the orthogonal [001] (or x) direction it is more or less constant, in accordance with the form of the Dresselhaus term (6).

Similar to the studies by Walser *et al.* (2012) on [001] quantum wells, Chen *et al.* (2014) also mapped out the formation of a helical spin structure following a local injection of spin density polarized along the growth direction. As this direction coincides with the direction of the spin-orbit field, an additional small magnetic field was necessary to generate nontrivial dynamics. Figure 8 shows the time-resolved data which is well reproduced by Monte Carlo simulations.

2. [111] quantum wells

According to Eqs. (7) and (8), the linear Dresselhaus coupling in quantum wells grown in the [111] direction can exactly cancel the Rashba term for $\alpha = 2\beta/\sqrt{3}$. Thus spin-orbit interaction is present only in higher corrections, the leading one being a third-harmonic contribution in Eq. (7). This situation in GaAs quantum wells was investigated by Balocchi *et al.* (2011) using time-resolved photoluminescence spectroscopy. For an appropriate Rashba coupling tuned by a gate voltage, they observed clearly enhanced spin lifetimes exceeding 30 ns for all spin directions. Spin polarizations perpendicular to the growth direction were generated by a transverse magnetic field of the order of a few hundred mT. In a subsequent work, Ye *et al.* (2012) found, for structures used by Balocchi *et al.* (2011), the sign of the gate voltage depends on whether the underlying GaAs [111] substrate is terminated by a $[111]A$ (Ga-rich) or a $[111]B$ (As-rich) surface.

Independent confirmation for these findings was provided by Biermann *et al.* (2012) and Hernandez-Minguez *et al.*

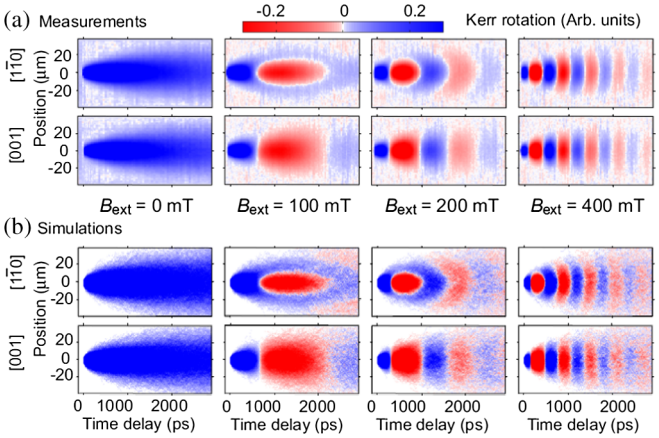

FIG. 8. Upper panels (a) Time- and spatially resolved Kerr rotation data by Chen *et al.* (2014). The dynamics of an initial spin polarization along the [110] growth direction is followed along the $[1\bar{1}0]$ and [001] directions. To generate nontrivial dynamics a magnetic field B_{ext} of various strength is applied along $[1\bar{1}0]$. Lower panels (b) Corresponding Monte Carlo simulation results. From Chen *et al.*, 2014.

(2012) who performed photoluminescence measurements on GaAs [111] quantum wells of somewhat larger width; for a summary, see also Hernandez-Minguez *et al.* (2014). Wang *et al.* (2013) recorded both the spin lifetime τ_s and the momentum relaxation time τ in GaAs [111] quantum wells and deduced an enhanced spin diffusion length $l_s = \sqrt{D\tau_s}$, $D = v_f^2\tau/2$, at an appropriate gate voltage. Moreover, Balocchi *et al.* (2013) combined optical experiments and theoretical simulations to investigate the influence of the cubic third-harmonic contribution to the Dresselhaus coupling close to the cancellation of the linear part with the Rashba term. They concluded that effective control over spin relaxation even at room temperature should be possible in sufficiently narrow [111] wells where the linear Dresselhaus term dominates.

3. Curved systems

Another situation where, for appropriately tuned spin-orbit interaction, nontrivial conserved spin quantities occur is realized by evenly curved cylindrical two-dimensional electron systems. The geometry of such samples is sketched in Fig. 9(a); for the practical fabrication of such structures see, e.g., Schmidt and Eberl (2001) and Mendach *et al.* (2004, 2006).

Including Rashba spin-orbit coupling, the Hamiltonian can be formulated as (Trushin and Schliemann, 2007b)

$$\mathcal{H} = \frac{\hbar^2 k_z^2}{2m} + \frac{\hbar^2 q_\varphi^2}{2mR^2} + \alpha\left(k_z\sigma^\varphi - \frac{q_\varphi}{R}\sigma^z\right), \tag{39}$$

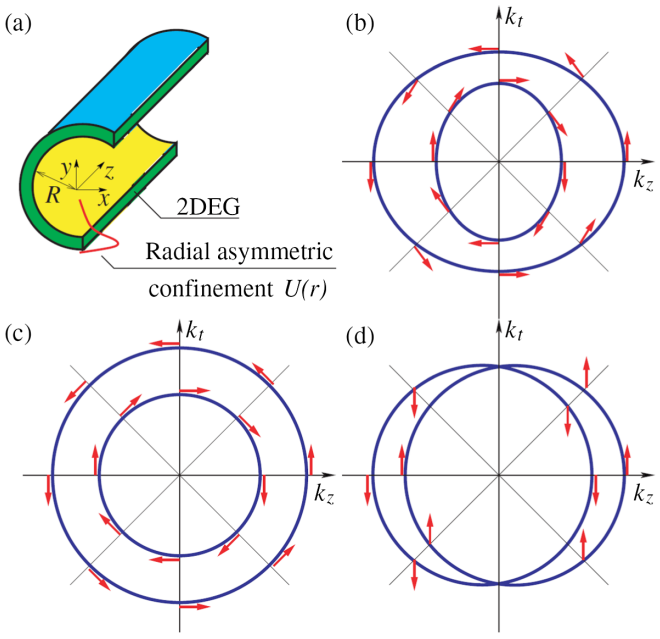

FIG. 9. (a) Sketch of a curved two-dimensional electron system with Rashba spin-orbit coupling induced by asymmetric radial confinement. (b) General case: Spin-orbit interaction leads to anisotropic Fermi contours ($k_t = q_\varphi$, spin direction given by arrows). (c) Isotropic Fermi contours of a *flat* system with Rashba coupling [cf. Eq. (8)]. (d) Fermi contours of the curved system with Rashba coupling tuned according to Eq. (41): Two circles displaced by a shift vector. From Trushin and Schliemann, 2007b.

where k_z is the wave vector component along the (z) axis of the cylinder of radius R, and $q_\varphi = -i\partial/\partial\varphi$ generates real-space rotations around the axis. $\sigma^\varphi = -\sigma^x \sin\varphi + \sigma^y \cos\varphi$ is the projection of the Pauli matrices on the azimuthal direction such that $[\sigma^\varphi, \sigma^z]/(2i) = \sigma^x \cos\varphi + \sigma^y \sin\varphi =: \sigma^r$. For a general Rashba parameter α the Hamiltonian (39) leads to anisotropic dispersions shown in Fig. 9(b), which differ from the case of a flat system described by the Hamiltonian (8) and depicted in Fig. 9(c).

One easily finds the commutator

$$[\mathcal{H}, \sigma^\varphi] = \left(\frac{\hbar^2}{2mR^2} + \frac{\alpha}{R}\right)(q_\varphi\sigma^r + \sigma^r q_\varphi), \tag{40}$$

which vanishes if the Rashba parameter fulfills

$$\alpha = -\frac{\hbar^2}{2mR}, \tag{41}$$

a result that remains valid if arbitrary spin-independent potentials or interactions are added to the Hamiltonian (39). Moreover, in full analogy to flat quantum wells with appropriately tuned Rashba and Dresselhaus parameters, the conservation of $\Sigma = \sigma^\varphi$ leads to circular dispersion relations displaced by a shift vector [cf. Fig. 9(d)]. Thus, analogous to Eqs. (23) and (24), we have a complete su(2) algebra of operators commuting with the Hamiltonian (Trushin and Schliemann, 2007b). Finally, the corresponding persistent spin structure can also be described via appropriate spin diffusion equations (Kleinert and Bryksin, 2009).

Independently of the condition (41) the Hamiltonian (39) always commutes with the total angular momentum $j = q_\varphi + \sigma^z/2$, and electrons in superpositions with the same j but opposite spin orientation show interesting periodic spin patterns along the cylindrical axis (Bringer and Schäpers, 2011).

As a somewhat related geometry, Nowak and Szafran (2009) studied circular quantum rings embedded in [001] quantum wells with Rashba and Dresselhaus spin-orbit couplings. Here the latter leads, except for the high-symmetry case $\alpha = \pm\beta$, to elliptical deformations of the confined electron density.

4. Lateral confinement, magnetic fields, and finite well width

Duckheim, Maslov, and Loss (2009) performed a theoretical study of the dynamical spin Hall effect (Duckheim and Loss, 2007) in a two-dimensional electron gas confined to a channel of finite width. Specifically, the spin accumulation at the channel boundary in response to an ac electric field along the channel direction was investigated. This effect is found to typically decay on the length scale set by the spin-orbit coupling. However, considering additionally a dc in-plane magnetic field at balanced spin-orbit coupling $\alpha = \pm\beta$ they were able to identify conditions under which such spatially oscillating spin profiles can extend over the entire channel, thus forming a driven spin helix.

Badalyan and Fabian (2010) studied the interplay between Rashba and Dresselhaus spin-orbit couplings at $\alpha = \pm\beta$ with a magnetic field in the growth direction of the quantum well,

and a hard-wall boundary oriented in either the direction of $\vec{Q}$ [cf. Eq. (12)] or perpendicular to it. In the former case a spin helix along the boundary arises. The key observation here is that the transformation (17) still yields a spin-independent Schrödinger equation (18) even if an arbitrary vector potential $\vec{A}(\vec{r})$ is coupled to the momentum $\vec{p} = -i\hbar\nabla \mapsto \vec{p} + e\vec{A}$, leading to a magnetic field $\vec{B}(\vec{r}) = \nabla \times \vec{A}(\vec{r})$ whose direct Zeeman coupling to the spin is neglected [as done by Badalyan and Fabian (2010)] such that Σ remains a conserved quantity.

Introducing further lateral confinement in a given quantum well constrains the electron motion to take place mainly in the direction along the boundary. An extreme case of such a situation is a (quasi-)one-dimensional quantum wire with only the lowest subband being occupied. However, even in broader channels the longitudinal component of the wave vector clearly dominates the dynamics. This constraint fixes the projection of the spin operator acting predominantly on the electron via spin-orbit interaction. As a result, the Dyakonov-Perel spin relaxation mechanism can be expected to be strongly suppressed by such lateral confinement. This effect is rather independent of particular tuning of spin-orbit coupling parameters, but as it clearly leads to enhanced spin lifetimes we also summarize the pertaining developments here; for further discussion, see also Holleitner (2011).

Following several quantitative theoretical predictions (Bournel *et al.*, 1998; Kiselev and Kim, 2000a; Mal'shukov and Chao, 2000; Pareek and Bruno, 2002), this suppression of spin relaxation in narrow channels was experimentally verified by Holleitner *et al.* (2006, 2007) combining time-resolved Faraday rotation measurements with evaluations of Shubnikov–de Haas oscillations. Their work was qualitatively confirmed by Kwon *et al.* (2007) also relying on the Shubnikov–de Haas effect. At about the same time, the crossover from two- to one-dimensional spin relaxation behavior was also found by Schäpers *et al.* (2006) and Wirthmann *et al.* (2006) via weak antilocalization studies.

Regarding the influence of a magnetic field in two-dimensional bulk systems at $\alpha = \pm\beta$, Wilde and Grundler (2013) predicted the disappearance of additional beatings in de Haas–van Alphen oscillations, an effect similar to the suppression of Zitterbewegung (Schliemann, Loss, and Westervelt, 2006; Biswas and Ghosh, 2012; Nita *et al.*, 2012).

Kunihashi, Kohda, and Nitta (2009) performed magnetoconductance measurements in narrow InGaAs wires with Rashba and Dresselhaus spin-orbit couplings tuned close to $\alpha = \pm\beta$. Here essentially weak localization is found since the spin relaxation length systematically exceeds the inelastic scattering length due to the combined effect of spatial dimension and the conserved spin quantity. In a subsequent study they investigated a semiclassical model for spin relaxation in systems with a focus on $\alpha = \pm\beta$, also proposing a method to quantitatively estimate the spin-orbit parameters (Kunihashi, Kohda, and Nitta, 2012). The most recent experimental work includes an investigation by Altmann *et al.* (2014) on quantum wires close to $\alpha = \beta$ (cf. Sec. II.D.1) and a Kerr rotation study of channels with dominating Dresselhaus coupling (Altmann *et al.*, 2015).

Also working close to the one-dimensional limit, Krstajic, Rezasoltani, and Vasilopoulos (2010) performed a theoretical study of the conductance of quantum wires in [001] wells with spatially varying Rashba and Dresselhaus couplings around $\alpha = \beta$ taking into account subband mixing. Further theoretical investigations considered spin-helical structures in quantum wires of finite length in the presence of Rashba coupling (Slipko and Pershin, 2011; Slipko, Savran, and Pershin, 2011; Slipko, Hayeva, and Pershin, 2013).

Fu and Egues (2015) theoretically studied the spin-orbit interaction in [001] quantum wells that were broad enough such that, for typical densities, the two lowest subbands $i = 1$, 2 are occupied in the ground state (Bernardes *et al.*, 2007). Treating interaction effects within the Hartree approximation and solving the resulting coupled Schrödinger-Poisson system, they obtained separate coefficients α_1, α_2 and β_1, β_2 for the Rashba and Dresselhaus couplings for each subband. Points of enhanced symmetry such as $\alpha_1 = \beta_1$ are discussed in more detail. Working upon these findings Fu *et al.* (2016) concluded that the coupling parameters can be tuned to be of equal modulus in each subband but with a different relative sign $\alpha_1 = \beta_1$, $\alpha_2 = -\beta_2$. This situation gives rise to a superposition of two persistent spin helices with orthogonal wave vectors leading to a *persistent skyrmion lattice*. Moreover, Wang, Li, and Fu (2015) discussed the possibility of a persistent spin helix in coupled double and triple GaAs quantum wells.

Nakhmedov and Alekperov (2012) considered electrons subjected to Rashba and Dresselhaus couplings near $\alpha = \beta$ and an in-plane magnetic field in quantum wells of finite thickness where the specific form of the transverse potential was taken into account. Moreover, Nazmitdinov, Pichugin, and Valín-Rodríguez (2009) investigated quantum wires with Rashba and Dresselhaus couplings of arbitrary strength where an in-plane magnetic field gives rise to a conserved spin operator for electrons with appropriate longitudinal momentum.

G. Spin field-effect transistors and related concepts

We now summarize recent developments regarding spin field-effect transistors relation to persistent spin structures. For a more comprehensive review on spin-transistor devices, see Sugahara and Nitta (2010). We mainly concentrate on [001] quantum wells.

In the classic proposal of a spin field-effect transistor due to Datta and Das (1990) already sketched in Fig. 2, an electron is emitted from a spin-polarized electrode into a semiconductor region where its spin is rotated via electrically tunable Rashba coupling. Depending on the rotation angle and the spin polarization of the detecting electrode, the electron passes through the device with a high or low probability, defining the "on" and "off" states of the transistor. Problems with this concept include the spin injection into the active semiconductor region (Schmidt *et al.*, 2000) and the randomization of spins due to scattering on imperfections as already discussed in Sec. II.B (Dyakonov and Perel, 1972). Indeed, so far these obstacles limit the signal efficiency in practical implementations to a rather low level (Koo *et al.*, 2009).

A means to tackle the issue of spin decay in [001] grown structures is to balance the Dresselhaus and Rashba couplings in one of the operational states of the transistor (Cartoixa, Ting, and Chang, 2003; Schliemann, Egues, and Loss, 2003). For example, the on state can be defined by $\alpha = \pm\beta$ such that the electron spin is symmetry protected, whereas in the off state $|\alpha| \neq \beta$ and spin randomization sets in. To fully exploit the spin conservation in the on state, it is useful to precisely define the locations of spin injection and detection by means of quantum point contacts (Schliemann, Egues, and Loss, 2003; Chuang *et al.*, 2015). Kunihashi *et al.* (2012) discussed a device operating between the states $\alpha = +\beta$ and $\alpha = -\beta$ (Schliemann, Egues, and Loss, 2003); for a recent experimental realization of such a scenario, see Yoshizumi *et al.* (2016). A variant of these concepts for [110] structures was put forward by Hall *et al.* (2003), where in one of the device states additional Rashba coupling leads to spin decoherence. Further theoretical proposals involving spatially inhomogeneous Rashba coupling include work by Liu, Chan, and Wang (2012) and Alomar, Serra, and Sanchez (2015).

In a proposal by Betthausen *et al.* (2012) electron spins are modulated adiabatically in the on state of the device (and therefore protected against decay), while in the off state diabatic Landau-Zener transitions induced by a spatially rotating magnetic field set in leading to spin decoherence. The feasibility of this device is demonstrated experimentally using a (Cd,Mn)Te diluted semiconductor quantum well (Betthausen *et al.*, 2012); for related theoretical work, see also Saarikoski, Dollinger, and Richter (2012) and Wojcik and Adamowski (2016).

Wunderlich *et al.* (2010) combined the spin field-effect transistor concept with the spin Hall effect in an *n*-doped GaAs quantum well. Spins are injected optically, and the conductance of the device is switched via a top gate. The spin polarization of the resulting current is detected via a transversal voltage resulting from the (inverse) spin Hall effect.

III. *p*-DOPED STRUCTURES, TOPOLOGICAL INSULATORS, AND OTHER SYSTEMS

As sketched in Fig. 1, the structure of the *p*-type valence band of III-V zinc-blende semiconductors is much richer compared to the *s*-type conduction band (Winkler, 2003; Fabian *et al.*, 2007; Korn, 2010; Wu, Jiang, and Weng, 2010; Yu and Cardona, 2010). A realistic band structure model consists here of the classic Luttinger Hamiltonian parametrizing the different masses for heavy and light holes (Luttinger, 1956) and an additional spin-orbit coupling contribution arising from structure- and bulk-inversion asymmetry (Winkler, 2003). The latter terms are analogous to the Rashba and Dresselhaus couplings for conduction band electrons. In particular, as pointed out only quite recently, in two-dimensional quantum wells pronounced Dresselhaus contributions, being linear in the in-plane momentum, can arise from the heavy and light hole mixing induced by boundary conditions at the nanostructure interfaces (Luo *et al.*, 2010; Durnev, Glazov, and Ivchenko, 2014). Taking into account these findings, Wenk, Kammermeier, and Schliemann (2016) identified conditions for strained *p*-doped [001] wells under which conserved spin quantities occur for holes being close to the Fermi contour. The latter is for realistic parameters well approximated by a circle. The circumstance that spin conservation here only applies to charge carriers with wave numbers close to k_f is similar to the result by Nazmitdinov, Pichugin, and Valín-Rodríguez (2009) who found conserved spin operators in *n*-doped quantum wires arising for appropriate wave vectors only. Wenk, Kammermeier, and Schliemann (2016) considered strained quantum wells with ground states being both of heavy and light hole types; more special results apply to unstrained systems. Similar conserved spin quantities in strained quantum wells were also found by Dollinger *et al.* (2014) and Sacksteder and Bernevig (2014) using band structure models where the linear Dresselhaus term plays a less dominant role. The spin conservation here is again restricted to a vicinity of the Fermi contour, but the necessary conditions on band structure parameters are difficult to meet in realistic materials.

Absor *et al.* (2015) performed *ab initio* calculations for wurtzite ZnO surfaces of appropriate orientation and predicted an effective spin splitting similar to Dresselhaus coupling in *n*-doped [110] quantum wells of zinc-blende materials [cf. Eq. (6)], which should analogously give rise to a persistent spin helix.

The possibility to realize persistent spin textures in monolayers of group-III metal monochalcogenides was discussed by Li and Appelbaum (2015).

Sacksteder *et al.* (2012) investigated spin conduction in surface states of three-dimensional topological insulators with anisotropic dispersion. The authors predicted coherent spin transport if (i) the effective Hamiltonian is tuned to conserve an appropriate spin component (such that its Dirac cone is infinitely stretched), or (ii) the Fermi energy is aligned with a local extremum of the anisotropic two-dimensional dispersion.

Liu, Jain, and Liu (2014) studied the proximity effect in layered structures of triplet superconductors and [001] semiconductor quantum wells with Rashba and Dresselhaus spin-orbit couplings. They concluded that the vector of triplet pair expectation values should form a long-ranged helix in the semiconductor material for $\alpha = \pm\beta$. Related Josephson effects and possible experimental setups are also discussed.

Yet another fascinating perspective is the possibility to realize persistent helical spin structures in systems of ultracold fermionic atoms as discussed by Tokatly and Sherman (2013).

IV. CONCLUSIONS AND OUTLOOK

We reviewed the gamut of developments related to the persistent spin helix that have emerged from the theoretical predictions by Schliemann, Egues, and Loss (2003) and Bernevig, Orenstein, and Zhang (2006). The topic is still a hot one as one can see from the list of references, a substantial amount of which date from the last two years. In particular, new experimental studies continue to appear.

Our discussion includes *n*-doped III-V zinc-blende quantum wells of growth directions [001], [110], and [111]. The first one has received the most attention so far, in both experimental and theoretical works. Right from the beginning the investigations about conserved spin operators and suppressed decoherence were closely tied to proposals for

improving the device concept of spin field-effect transistors. Among the most promising experimental developments in this regard are the very recent studies on drift transport of spin helices as discussed in Sec. II.D.1. It is needless to say that these achievements have the chance to contribute to spin-based information processing in semiconductor structures.

Systems with growth directions [110] and [111] have also been subject to thorough experimental studies, while the predicted many-body effects of persistent spin textures (mainly in [001] quantum wells) are still awaiting their experimental investigation.

A most recent theoretical result was obtained by Kammermeier, Wenk, and Schliemann (2016) stating that a persistent spin helix is achievable in quantum wells of more general growth direction if and only if two of its Miller indices have the same modulus. Specifically, the resulting SU(2) symmetry is characterized by a conserved spin component $\Sigma = \vec{e} \cdot \vec{\sigma}$ and a shift vector $\vec{Q}$, which is always perpendicular to the direction of the spin-orbit field $\vec{e} \perp \vec{Q}$. The latter feature is strongly reminiscent of the spin-momentum locking found in the edge modes of topological insulators (Hasan and Kane, 2010; Qi and Zhang, 2011) but occurs here in the bulk of the system. These findings have the potential to stimulate a flurry of further fascinating experiments.

Other recent developments include the study of two-dimensional *p*-doped systems, which are well known for their clearly richer band structure.

ACKNOWLEDGMENTS

I thank E. Bernardes, G. Burkard, T. Dollinger, J. C. Egues, S. I. Erlingsson, S. D. Ganichev, M. S. Garelli, M. Kammermeier, M. Lee, D. Loss, K. Richter, D. Saraga, A. Scholz, M. Trushin, P. Wenk, R. M. Westervelt, and R. Winkler for collaborations on topics related to this article. Moreover, I am grateful to J. Fabian, S. D. Ganichev, J. Nitta, J. Orenstein, K. Richter, G. Salis, and D. Weiss for permission to reproduce figures from their publications. Thanks for useful comments on the manuscript go to P. Wenk. This work was supported by the Deutsche Forschungsgemeinschaft via SFB 689.

REFERENCES

Absor, M. A. U., F. Ishii, H. Kotaka, and M. Saito, 2015, Appl. Phys. Express **8**, 073006.
Alomar, M. I., L. Serra, and D. Sanchez, 2015, arXiv:1512.05958.
Altmann, P., F. G. G. Hernandez, G. J. Ferreira, M. Kohda, C. Reichl, W. Wegscheider, and G. Salis, 2016, Phys. Rev. Lett. **116**, 196802.
Altmann, P., M. Kohda, C. Reichl, W. Wegscheider, and G. Salis, 2015, Phys. Rev. B **92**, 235304.
Altmann, P., M. P. Walser, C. Reichl, W. Wegscheider, and G. Salis, 2014, Phys. Rev. B **90**, 201306.
Averkiev, N. S., and L. E. Golub, 1999, Phys. Rev. B **60**, 15582.
Badalyan, S. M., and J. Fabian, 2010, Phys. Rev. Lett. **105**, 186601.
Badalyan, S. M., A. Matos-Abiague, J. Fabian, G. Vignale, and F. M. Peeters, 2013, Phys. Rev. B **88**, 195402.
Badalyan, S. M., A. Matos-Abiague, G. Vignale, and J. Fabian, 2009, Phys. Rev. B **79**, 205305.
Badalyan, S. M., A. Matos-Abiague, G. Vignale, and J. Fabian, 2010, Phys. Rev. B **81**, 205314.
Balocchi, A., T. Amand, G. Wang, B. L. Liu, P. Renucci, Q. H. Duong, and X. Marie, 2013, New J. Phys. **15**, 095016.
Balocchi, A., Q. H. Duong, P. Renucci, B. L. Liu, C. Fontaine, T. Amand, D. Lagarde, and X. Marie, 2011, Phys. Rev. Lett. **107**, 136604.
Bel'kov, V. V., P. Olbrich, S. A. Tarasenko, D. Schuh, W. Wegscheider, T. Korn, C. Schüller, D. Weiss, W. Prettl, and S. D. Ganichev, 2008, Phys. Rev. Lett. **100**, 176806.
Bernardes, E., J. Schliemann, M. Lee, J. C. Egues, and D. Loss, 2007, Phys. Rev. Lett. **99**, 076603.
Bernevig, B. A., and J. Hu, 2008, Phys. Rev. B **78**, 245123.
Bernevig, B. A., J. Orenstein, and S.-C. Zhang, 2006, Phys. Rev. Lett. **97**, 236601.
Betthausen, C., T. Dollinger, H. Saarikoski, V. Kolkovsky, G. Karczewski, T. Wojtowicz, K. Richter, and D. Weiss, 2012, Science **337**, 324.
Biermann, K., A. Hernandez-Minguez, R. Hey, and P. V. Santos, 2012, J. Appl. Phys. **112**, 083913.
Bindel, J. R., M. Pezzotta, J. Ulrich, M. Liebmann, E. Sherman, and M. Morgenstern, 2016, Nat. Phys. **12**, 920.
Biswas, T., and T. K. Ghosh, 2012, J. Phys. Condens. Matter **24**, 185304.
Bjorken, J. D., and S. D. Drell, 1965, *Relativistic Quantum Mechanics* (McGraw-Hill, New York).
Bournel, A., P. Dollfus, P. Bruno, and P. Hesto, 1998, Eur. Phys. J. Appl. Phys. **4**, 1.
Bringer, A., and T. Schäpers, 2011, Phys. Rev. B **83**, 115305.
Burkov, A. A., A. S. Núñez, and A. H. MacDonald, 2004, Phys. Rev. B **70**, 155308.
Bychkov, Y. A., and E. I. Rashba, 1984, JETP Lett. **39**, 78.
Capps, J., D. C. Marinescu, and A. Manolescu, 2015, Phys. Rev. B **91**, 165301.
Capps, J., D. C. Marinescu, and A. Manolescu, 2016, Phys. Rev. B **93**, 085307.
Cartoixa, X., D. Z.-Y. Ting, and Y.-C. Chang, 2003, Appl. Phys. Lett. **83**, 1462–1464.
Cartoixa, X., D. Z.-Y. Ting, and Y.-C. Chang, 2005a, J. Supercond. **18**, 163.
Cartoixa, X., D. Z.-Y. Ting, and Y.-C. Chang, 2005b, Phys. Rev. B **71**, 045313.
Chalaev, O., and D. Loss, 2008, Phys. Rev. B **77**, 115352.
Chalaev, O., and D. Loss, 2009, Phys. Rev. B **80**, 035305.
Chen, S.-H., and C.-R. Chang, 2008, Phys. Rev. B **77**, 045324.
Chen, Y. S., S. Fält, W. Wegscheider, and G. Salis, 2014, Phys. Rev. B **90**, 121304.
Cheng, J. L., and M. W. Wu, 2006, J. Appl. Phys. **99**, 083704.
Cheng, J. L., M. W. Wu, and I. C. da Cunha Lima, 2007, Phys. Rev. B **75**, 205328.
Chesi, S., and D. Loss, 2010, Phys. Rev. B **82**, 165303.
Chuang, P., *et al.*, 2015, Nat. Nanotechnol. **10**, 35.
Couto, O. D. D., F. Iikawa, J. Rudolph, R. Hey, and P. V. Santos, 2007, Phys. Rev. Lett. **98**, 036603.
Darnhofer, T., and U. Rössler, 1993, Phys. Rev. B **47**, 16020.
Datta, S., and B. Das, 1990, Appl. Phys. Lett. **56**, 665.
de Andrada e Silva, E. A., G. C. La Rocca, and F. Bassani, 1997, Phys. Rev. B **55**, 16293.
Denega, S. Z., T. Last, J. Liu, A. Slachter, P. J. Rizo, P. H. M. van Loosdrecht, B. J. van Wees, D. Reuter, A. D. Wieck, and C. H. van der Wal, 2010, Phys. Rev. B **81**, 153302.
Dettwiler, F., J. Fu, S. Mack, P. J. Weigele, J. C. Egues, D. D. Awschalom, and D. M. Zumbuhl, 2014, arXiv:1403.3518.
Döhrmann, S., D. Hägele, J. Rudolph, M. Bichler, D. Schuh, and M. Oestreich, 2004, Phys. Rev. Lett. **93**, 147405.

Dollinger, T., M. Kammermeier, A. Scholz, P. Wenk, J. Schliemann, K. Richter, and R. Winkler, 2014, Phys. Rev. B **90**, 115306.

Dresselhaus, G., 1955, Phys. Rev. **100**, 580.

Duckheim, M., and D. Loss, 2007, Phys. Rev. B **75**, 201305.

Duckheim, M., D. L. Maslov, and D. Loss, 2009, Phys. Rev. B **80**, 235327.

Durnev, M. V., M. M. Glazov, and E. L. Ivchenko, 2014, Phys. Rev. B **89**, 075430.

Dyakonov, M. I., and V. Y. Kachorovskii, 1986, Sov. Phys. Semicond. **20**, 110.

Dyakonov, M. I., and V. I. Perel, 1972, Sov. Phys. Solid State **13**, 3023.

Eppenga, R., and M. F. H. Schuurmans, 1988, Phys. Rev. B **37**, 10923.

Erlingsson, S. I., J. Schliemann, and D. Loss, 2005, Phys. Rev. B **71**, 035319.

Fabian, J., 2009, Nature (London) **458**, 580.

Fabian, J., A. Matos-Abiague, C. Ertler, P. Stano, and I. Zutic, 2007, Acta Phys. Slovaca **57**, 565.

Fu, J., and J. C. Egues, 2015, Phys. Rev. B **91**, 075408.

Fu, J., P. H. Penteado, M. O. Hachiya, D. Loss, and J. C. Egues, 2016, Phys. Rev. Lett. **117**, 226401.

Ganichev, S. D., and L. E. Golub, 2014, Phys. Status Solidi (b) **251**, 1801–1823.

Ganichev, S. D., *et al.*, 2004, Phys. Rev. Lett. **92**, 256601.

Glazov, M., E. Sherman, and V. Dugaev, 2010, Physica E (Amsterdam) **42**, 2157.

Glazov, M. M., M. A. Semina, and E. Y. Sherman, 2010, Phys. Rev. B **81**, 115332.

Griesbeck, M., M. M. Glazov, E. Y. Sherman, D. Schuh, W. Wegscheider, C. Schüller, and T. Korn, 2012, Phys. Rev. B **85**, 085313.

Hall, K. C., W. H. Lau, K. Gundogdu, M. E. Flatte, and T. F. Boggess, 2003, Appl. Phys. Lett. **83**, 2937.

Hasan, M. Z., and C. L. Kane, 2010, Rev. Mod. Phys. **82**, 3045.

Hernandez-Minguez, A., K. Biermann, R. Hey, and P. V. Santos, 2012, Phys. Rev. Lett. **109**, 266602.

Hernandez-Minguez, A., K. Biermann, R. Hey, and P. V. Santos, 2014, Phys. Status Solidi (b) **251**, 1736–1752.

Holleitner, A. W., 2011, *CFN Lectures on Functional Nanostructures —Volume 2: Nanoelectronics* (Springer, Berlin/Heidelberg), p. 145.

Holleitner, A. W., V. Sih, R. C. Myers, A. C. Gossard, and D. D. Awschalom, 2006, Phys. Rev. Lett. **97**, 036805.

Holleitner, A. W., V. Sih, R. C. Myers, A. C. Gossard, and D. D. Awschalom, 2007, New J. Phys. **9**, 342.

Iglesias, P. E., and J. A. Maytorena, 2010, Phys. Rev. B **82**, 205324.

Iordanskii, S. V., Y. B. Lyanda-Geller, and G. E. Pikus, 1994, JETP Lett. **60**, 206.

Ishihara, J., Y. Ohno, and H. Ohno, 2014a, Appl. Phys. Express **7**, 013001.

Ishihara, J., Y. Ohno, and H. Ohno, 2014b, Jpn. J. Appl. Phys. **53**, 04EM04.

Kalevich, V., V. Korenev, and I. Merkulov, 1994, Solid State Commun. **91**, 559.

Kammermeier, M., P. Wenk, and J. Schliemann, 2016, Phys. Rev. Lett. **117**, 236801.

Kettemann, S., 2007, Phys. Rev. Lett. **98**, 176808.

Kiselev, A. A., and K. W. Kim, 2000a, Phys. Rev. B **61**, 13115.

Kiselev, A. A., and K. W. Kim, 2000b, Phys. Status Solidi (b) **221**, 491–494.

Kleinert, P., and V. V. Bryksin, 2007, Phys. Rev. B **76**, 205326.

Kleinert, P., and V. V. Bryksin, 2009, Phys. Rev. B **79**, 045317.

Knap, W., *et al.*, 1996, Phys. Rev. B **53**, 3912.

Kohda, M., *et al.*, 2012, Phys. Rev. B **86**, 081306.

Koo, H. C., J. H. Kwon, J. Eom, J. Chang, S. H. Han, and M. Johnson, 2009, Science **325**, 1515.

Koralek, J. D., C. P. Weber, J. Orenstein, B. A. Bernevig, S.-C. Zhang, S. Mack, and D. D. Awschalom, 2009, Nature (London) **458**, 610.

Korn, T., 2010, Phys. Rep. **494**, 415.

Krstajic, P. M., E. Rezasoltani, and P. Vasilopoulos, 2010, Phys. Rev. B **81**, 155325.

Kunihashi, Y., M. Kohda, and J. Nitta, 2009, Phys. Rev. Lett. **102**, 226601.

Kunihashi, Y., M. Kohda, and J. Nitta, 2012, Phys. Rev. B **85**, 035321.

Kunihashi, Y., M. Kohda, H. Sanada, H. Gotoh, T. Sogawa, and J. Nitta, 2012, Appl. Phys. Lett. **100**, 113502.

Kunihashi, Y., H. Sanada, H. Gotoh, K. Onomitsu, M. Kohda, J. Nitta, and T. Sogawa, 2016, Nat. Commun. **7**, 10722.

Kurosawa, R., K. Morita, M. Kohda, and Y. Ishitani, 2015, Appl. Phys. Lett. **107**, 182103.

Kwon, J. H., H. C. Koo, J. Chang, S.-H. Han, and J. Eom, 2007, Appl. Phys. Lett. **90**, 112505.

Li, J., and K. Chang, 2010, Phys. Rev. B **82**, 033304.

Li, P., and I. Appelbaum, 2015, Phys. Rev. B **92**, 195129.

Li, Z., F. Marsiglio, and J. P. Carbotte, 2013, Sci. Rep. **3**, 02828.

Liu, G. H., Y. H. Chen, C. H. Jia, and Z. G. Wang, 2009, Eur. Phys. J. B **70**, 397.

Liu, J., T. Last, E. J. Koop, S. Z. Denega, B. J. van Wees, and C. H. van der Wal, 2010, J. Supercond. Novel Magn. **23**, 11.

Liu, J.-F., K. S. Chan, and J. Wang, 2012, Appl. Phys. Lett. **101**, 082407.

Liu, M.-H., K.-W. Chen, S.-H. Chen, and C.-R. Chang, 2006, Phys. Rev. B **74**, 235322.

Liu, X., J. K. Jain, and C.-X. Liu, 2014, Phys. Rev. Lett. **113**, 227002.

Liu, X., and J. Sinova, 2012, Phys. Rev. B **86**, 174301.

Lopez-Bastidas, C., J. A. Maytorena, and F. Mireles, 2007, Phys. Status Solidi (c) **4**, 4229.

Lüffe, M. C., J. Danon, and T. S. Nunner, 2013, Phys. Rev. B **87**, 125416.

Lüffe, M. C., J. Kailasvuori, and T. S. Nunner, 2011, Phys. Rev. B **84**, 075326.

Luo, J.-W., A. N. Chantis, M. van Schilfgaarde, G. Bester, and A. Zunger, 2010, Phys. Rev. Lett. **104**, 066405.

Lusakowski, A., J. Wrobel, and T. Dietl, 2003, Phys. Rev. B **68**, 081201.

Luttinger, J. M., 1956, Phys. Rev. **102**, 1030.

Lyubinskiy, I. S., and V. Y. Kachorovskii, 2006, Phys. Rev. B **73**, 041301.

Mal'shukov, A. G., and K. A. Chao, 2000, Phys. Rev. B **61**, R2413.

Manchon, A., H. C. Koo, J. Nitta, S. M. Frolov, and R. A. Duine, 2015, Nat. Mater. **14**, 871.

Maytorena, J. A., C. Lopez-Bastidas, and F. Mireles, 2006, Phys. Rev. B **74**, 235313.

Mendach, S., O. Schumacher, C. Heyn, S. Schnüll, H. Welsch, and W. Hansen, 2004, Physica E (Amsterdam) **23**, 274.

Mendach, S., O. Schumacher, H. Welsch, C. Heyn, W. Hansen, and M. Holz, 2006, Appl. Phys. Lett. **88**, 212113.

Meng, T., J. Klinovaja, and D. Loss, 2014, Phys. Rev. B **89**, 205133.

Mishchenko, E. G., A. V. Shytov, and B. I. Halperin, 2004, Phys. Rev. Lett. **93**, 226602.

Müller, G. M., M. Römer, D. Schuh, W. Wegscheider, J. Hübner, and M. Oestreich, 2008, Phys. Rev. Lett. **101**, 206601.

Nakhmedov, E., and O. Alekperov, 2012, Eur. Phys. J. B **85**, 298.

Nazmitdinov, R. G., K. N. Pichugin, and M. Valín-Rodríguez, 2009, Phys. Rev. B **79**, 193303.
Nechaev, I. A., P. M. Echenique, and E. V. Chulkov, 2010, Phys. Rev. B **81**, 195112.
Nita, M., D. Marinescu, A. Manolescu, B. Ostahie, and V. Gudmundsson, 2012, Physica E (Amsterdam) **46**, 12.
Nowak, M. P., and B. Szafran, 2009, Phys. Rev. B **80**, 195319.
Ohno, M., and K. Yoh, 2007, Phys. Rev. B **75**, 241308.
Ohno, M., and K. Yoh, 2008, Phys. Rev. B **77**, 045323.
Ohno, Y., R. Terauchi, T. Adachi, F. Matsukura, and H. Ohno, 1999, Phys. Rev. Lett. **83**, 4196.
Pareek, T. P., and P. Bruno, 2002, Phys. Rev. B **65**, 241305.
Pikus, F. G., and G. E. Pikus, 1995, Phys. Rev. B **51**, 16928.
Poshakinskiy, A. V., and S. A. Tarasenko, 2013, Phys. Rev. B **87**, 235301.
Qi, X.-L., and S.-C. Zhang, 2011, Rev. Mod. Phys. **83**, 1057.
Raimondi, R., C. Gorini, P. Schwab, and M. Dzierzawa, 2006, Phys. Rev. B **74**, 035340.
Rashba, E. I., 1960, Sov. Phys. Solid State **2**, 1109.
Saarikoski, H., T. Dollinger, and K. Richter, 2012, Phys. Rev. B **86**, 165407.
Sacksteder, V. E., and B. A. Bernevig, 2014, Phys. Rev. B **89**, 161307.
Sacksteder, V. E., S. Kettemann, Q. Wu, X. Dai, and Z. Fang, 2012, Phys. Rev. B **85**, 205303.
Salis, G., M. P. Walser, P. Altmann, C. Reichl, and W. Wegscheider, 2014, Phys. Rev. B **89**, 045304.
Sasaki, A., S. Nonaka, Y. Kunihashi, M. Kohda, T. Bauernfeind, T. Dollinger, K. Richter, and J. Nitta, 2014, Nat. Nanotechnol. **9**, 703–709.
Schäpers, T., V. A. Guzenko, M. G. Pala, U. Zülicke, M. Governale, J. Knobbe, and H. Hardtdegen, 2006, Phys. Rev. B **74**, 081301.
Scheid, M., M. Kohda, Y. Kunihashi, K. Richter, and J. Nitta, 2008, Phys. Rev. Lett. **101**, 266401.
Schliemann, J., 2006, Int. J. Mod. Phys. B **20**, 1015.
Schliemann, J., J. C. Egues, and D. Loss, 2003, Phys. Rev. Lett. **90**, 146801.
Schliemann, J., and D. Loss, 2003, Phys. Rev. B **68**, 165311.
Schliemann, J., D. Loss, and R. M. Westervelt, 2006, Phys. Rev. B **73**, 085323.
Schmidt, G., D. Ferrand, L. W. Molenkamp, A. T. Filip, and B. J. van Wees, 2000, Phys. Rev. B **62**, R4790.
Schmidt, O. G., and K. Eberl, 2001, Nature (London) **410**, 168.
Schönhuber, C., M. P. Walser, G. Salis, C. Reichl, W. Wegscheider, T. Korn, and C. Schüller, 2014, Phys. Rev. B **89**, 085406.
Schreiber, L., D. Duda, B. Beschoten, G. Güntherodt, H.-P. Schönherr, and J. Herfort, 2007a, Phys. Rev. B **75**, 193304.
Schreiber, L., D. Duda, B. Beschoten, G. Güntherodt, H.-P. Schönherr, and J. Herfort, 2007b, Phys. Status Solidi (b) **244**, 2960.
Schwab, P., M. Dzierzawa, C. Gorini, and R. Raimondi, 2006, Phys. Rev. B **74**, 155316.
Shen, K., and M. Wu, 2009, J. Supercond. Novel Magn. **22**, 715.
Slipko, V. A., A. A. Hayeva, and Y. V. Pershin, 2013, Phys. Rev. B **87**, 035430.
Slipko, V. A., and Y. V. Pershin, 2011, Phys. Rev. B **84**, 155306.
Slipko, V. A., I. Savran, and Y. V. Pershin, 2011, Phys. Rev. B **83**, 193302.
Stanescu, T. D., and V. Galitski, 2007, Phys. Rev. B **75**, 125307.
Studer, M., G. Salis, K. Ensslin, D. C. Driscoll, and A. C. Gossard, 2009, Phys. Rev. Lett. **103**, 027201.
Sugahara, S., and J. Nitta, 2010, Proc. IEEE **98**, 2124.
Tarasenko, S., and N. Averkiev, 2002, JETP Lett. **75**, 552.
Tarasenko, S. A., 2009, Phys. Rev. B **80**, 165317.
Tokatly, I. V., and E. Y. Sherman, 2010, Phys. Rev. B **82**, 161305.
Tokatly, I. V., and E. Y. Sherman, 2013, Phys. Rev. A **87**, 041602.
Trushin, M., and J. Schliemann, 2007a, Phys. Rev. B **75**, 155323.
Trushin, M., and J. Schliemann, 2007b, New J. Phys. **9**, 346.
Völkl, R., M. Griesbeck, S. A. Tarasenko, D. Schuh, W. Wegscheider, C. Schüller, and T. Korn, 2011, Phys. Rev. B **83**, 241306.
Völkl, R., M. Schwemmer, M. Griesbeck, S. A. Tarasenko, D. Schuh, W. Wegscheider, C. Schüller, and T. Korn, 2014, Phys. Rev. B **89**, 075424.
Vurgaftman, I., and J. R. Meyer, 2005, J. Appl. Phys. **97**, 053707.
Walser, M. P., C. Reichl, W. Wegscheider, and G. Salis, 2012, Nat. Phys. **8**, 757.
Wang, G., B. L. Liu, A. Balocchi, P. Renucci, C. R. Zhu, T. Amand, C. Fontaine, and X. Marie, 2013, Nat. Commun. **4**, 2372.
Wang, W., X. Li, and J. Fu, 2015, Superlattices Microstruct. **88**, 43.
Wenk, P., M. Kammermeier, and J. Schliemann, 2016, Phys. Rev. B **93**, 115312.
Wenk, P., and S. Kettemann, 2010, Phys. Rev. B **81**, 125309.
Wenk, P., and S. Kettemann, 2011, Phys. Rev. B **83**, 115301.
Wilde, M. A., and D. Grundler, 2013, New J. Phys. **15**, 115013.
Winkler, R., 2003, *Spin-Orbit Coupling Effects in Two-Dimensional Eletron and Hole Systems*, Springer Tracts in Modern Physics, Vol. 191 (Springer, New York).
Wirthmann, A., Y. Gui, C. Zehnder, D. Heitmann, C.-M. Hu, and S. Kettemann, 2006, Physica E (Amsterdam) **34**, 493.
Wojcik, P., and J. Adamowski, 2016, Semicond. Sci. Technol. **31**, 035021.
Wu, M., J. Jiang, and M. Weng, 2010, Phys. Rep. **493**, 61.
Wunderlich, J., B.-G. Park, A. C. Irvine, L. P. Zrbo, E. Rozkotov, P. Nemec, V. Novk, J. Sinova, and T. Jungwirth, 2010, Science **330**, 1801.
Yang, L., J. D. Koralek, J. Orenstein, D. R. Tibbetts, J. L. Reno, and M. P. Lilly, 2012, Phys. Rev. Lett. **109**, 246603.
Yang, L., J. Orenstein, and D.-H. Lee, 2010, Phys. Rev. B **82**, 155324.
Ye, H. Q., *et al.*, 2012, Appl. Phys. Lett. **101**, 032104.
Yoshizumi, K., A. Sasaki, M. Kohda, and J. Nitta, 2016, Appl. Phys. Lett. **108**, 132402.
Yu, P., and M. Cardona, 2010, *Fundamentals of Semiconductors: Physics and Materials Properties, Graduate Texts in Physics* (Springer, New York).
Zutic, I., J. Fabian, and S. Das Sarma, 2004, Rev. Mod. Phys. **76**, 323.